CHALMERS
UNIVERSITY OF TECHNOLOGY

Modeling and control for object manipulation via in-hand pivoting

Master's thesis in Systems, Control and Mechatronics

Leon Amirpour

Department of Electrical Engineering
CHALMERS UNIVERSITY OF TECHNOLOGY
Gothenburg, Sweden 2017

Master's thesis Ex059/2017

Modeling and control for object manipulation via in-hand pivoting

LEON AMIRPOUR

CHALMERS
UNIVERSITY OF TECHNOLOGY

Department of Electrical Engineering
Division of Systems and Control
Chalmers University of Technology
Gothenburg, Sweden 2017

Modeling and control for object manipulation via in-hand pivoting
LEON AMIRPOUR

Supervisor and Examiner: Yiannis Karayiannidis, Assistant Professor, Department of Electrical Engineering, Chalmers University of Technology

Master's Thesis EX059/2017
Department of Electrical Engineering
Division of Systems and Control
Chalmers University of Technology
SE-412 96 Gothenburg
Telephone +46 31 772 1000

Typeset in LaTeX
Gothenburg, Sweden 2017

Modeling and control for object manipulation via in-hand pivoting
LEON AMIRPOUR
Department of Electrical Engineering
Chalmers University of Technology

Abstract

In this thesis in-hand manipulation maneuvers that consist of rotating and sliding of a grasped object to a desired orientation relative to the robot hand are simulated. We perform pivoting by means of gravity to allow the object grasped by a one degree of freedom gripper to follow a reference trajectory to a desired angular position by controlling the grasping force. The contact between the object and the gripper is modeled based on the concept of the limit surface, which describes the relation between rotational and translational friction torques and forces and the corresponding dynamics. The difficulty of controlling the object orientation is due to the uncertainty of the torsional friction coefficient. Two different control approaches are applied to deal with this problem. First, a nonlinear adaptive control approach is utilized, which allows to estimate the torsional friction coefficient on-line. Second, a model free control approach is used to exploit prescribed performance guarantees without exact knowledge of the plant. Both controllers are evaluated through simulation and show good results for a wide range of pivoting tasks.

Keywords: contact modeling, contact and friction dynamics, nonlinear and adaptive control, simulation, robotics, limit surface, model free control, prescribed performance.

Contents

List of Figures

List of Tables

1
Introduction

1.1 Context

Nowadays robots are used very frequently in production utilizing very simple grippers such as parallel jaw grippers or even suction cups. In contrast to robots, the human hand is capable to reposition the grasped object in the hand, by rolling, pushing or sliding of the object by coordinated motions of the fingers. The rather simple robotic grippers with only a few degrees of freedom cannot recreate the dexterity of the human hand. To compensate this lack of dexterity, extrinsic dexterity can be used. Extrinsic dexterity means to make use of external forces or contacts to enable the robot performing relevant manipulation tasks.
One basic scenario of in-hand manipulation is sliding and pivoting of the object in the hand with the help of the gravity of the object. More precisely, a one degree of freedom parallel jaw gripper can be appropriately controlled in order to allow or prevent the rotation of the object under the effect of the gravitational force. In such way, the orientation of the object can be controlled to a desired angular position.

1.2 Related work

There exists a considerable array of research work related to in-hand manipulation tasks. In [1] - [5] different examples have been shown how robots can make effective use of extrinsic dexterity for in-hand manipulation. Dafle and Rodriguez manipulate an object grasped by a parallel jaw gripper [1]. The object is manipulated through pushing it against its environment. Dafle et al. use a gripper with three rigid fingers to develop twelve open-loop and hand-scripted regrasp actions [2]. Gravitational forces and motions of the robot arm and fingers are exploited to achieve the desired motion of the object. Different open-loop pivoting experiments were made by Holladay et al. [3]. The regrasp processes are compared with pick-and-place operations, which lead to the same regrasping as the in-hand manipulation tasks. Pick-and-place in terms of regrasping means to put the grasped object on the ground and grasp it at another grasping point or with another orientation of the gripper. It was found that manipulating the object via pivoting can be faster than manipulation through pick-and-place. Shi et al. presented a general framework for planning dynamic in-hand manipulation and analyzed the dynamics of a grasp with n fingers modeled with the use of soft-finger limit surface models [4]. Dynamic in-hand manipulation with a constant normal force between the gripper and the object is performed. Through precise acceleration of the fingers the object is linear and rotational displaced. Viña

B. et al. developed a sliding mode controller for in-hand manipulations to control the orientation of the object by using gravity [5]. It is assumed that the grasping force of the parallel jaw gripper is big enough that no translational slippage appears. The frictional torque is modeled as a combined friction of Coulomb and viscous friction and the deformation model of the fingertips is assumed as linear.

The same scenario as in this project is presented in [6]. A one degree of freedom parallel jaw gripper is used and pivoting by means of gravity is performed. An adaptive controller controls the grasping force to ensure that the object follows a trajectory and arrives at the desired angular position. The result is evaluated in an actual robotic gripper using force and tactile sensors. For the control design in [6] the contact model between the hand and the object is based on Coulomb friction for the tangential friction and a Coulomb-like model [7], [8] for the torsional friction. The adaptive controller is derived with the standard adaptive control law [9]. Another control approach, which is suitable for this control problem, is considered in [10]. Karayiannidis et al. present a model free controller for a position and velocity tracking of a robot joint with prescribed performance guarantees.

To simulate in-hand manipulation, the contact between the gripper and the object has to be investigated. Liu et al. developed a novel contact sensing algorithm for a robotic fingertip in [11]. Validation tests show that the contact sensing fingertip can estimate contact information, such as the magnitude and the direction of the friction force and local torque generated at the surface and the contact location on the fingertip. Xydas and Kao show the relationship between the normal force and the radius of contact for soft fingers [8]. General soft-finger materials are considered, including linearly and nonlinearly elastic materials. It is shown that the radius of the contact area is proportional to the normal force raised to the power of γ, where γ has the range from 0 to 1/3.

A contact friction model between the fingertips of the gripper and the object is needed to simulate in-hand pivoting and it is of interest which kind of model is suitable. In [12] a Coulomb friction model is derived and controlled with a PID controller. This model considers just the motion and the friction in one dimension. A dependency between translational and rotational dynamics of an object affected by friction is shown in [13] and [14]. An external torque reduces the static friction force, which has to be overcome for a contact sliding. To model a more dimensional contact friction model a limit surface can be used. The concept of the limit surface was developed by Goyal et al. in [15] and [16]. It is a concept from the mechanics of sliding bodies that uses kinematic analysis to find the force and moment required to produce any given sliding motion. The concept of the limit surface is used in [4] and [6] for in-hand manipulation tasks. The relationship between forces and motions in sliding manipulation with the help of limit surfaces is shown in [7].

1.3 Approach and Structure

In the presented thesis, a theoretical model is derived, which describes the contact between the fingertips of the gripper and the object. Using the concept of the limit surface allows to consider both translational and rotational motions of the object while pivoting. The credibility of the constructed model is tested through simulation, implementing the model in *MATLAB/SIMULINK*.
To control the orientation of the object in a desired way, an adaptive controller is designed. The adaptive controller estimates the torsional friction coefficient online to compensate for possible uncertainties. Another control approach, which is utilized to handle the uncertainties of the torsional friction coefficient, is a model free controller with prescribed performance guarantees. The performance of the controller is also validated through simulation.
The thesis is structured as follows: in Chapter 2 we introduce the theoretical background relevant for this thesis briefly. Chapter 3 provides the modeling of the object and the contact between the fingertips of the robot and the object. Also the models are evaluated by simulation and compared. The control problem and objectives are introduced briefly. In Chapter 4, different control approaches suitable for the pivoting task are derived. The results and comparisons of all models and controller are shown in Chapter 5. The models are evaluated via simulation of several scenarios. Conclusions are drawn and suggestions for future work are given in Chapter 6.

2

Background

In this section, the theoretical background relevant for this thesis is introduced briefly. For the notation convention, time dependencies are generally dropped throughout the thesis whenever this enhances readability.

2.1 Contact model

A contact model describes the deformation and friction between solid objects that touch each other at one or several points.

2.1.1 Limit surface

The concept of the limit surface describes the relationship between translational and rotational friction forces and torques and the corresponding dynamics. It is a concept from the mechanics of sliding bodies that uses kinematic analysis to find the force and moment required to produce any given sliding motion.
The concept of the limit surface was developed by Goyal et al. in [15] and [16]. The construction of the limit surface requires an accurate analysis of the pressure distribution at each point of the contact surface and the contribution of each point to the total frictional force and moment.
Three basic assumptions were made:

1. The distribution of the normal force or pressure across the contact is known.
2. A body undergoes fully developed sliding on a locally planar surface.
3. The friction force depends only on the local normal force and direction of slip and not on the slip velocity or slip history.

To ensure the fully developed sliding criteria (2.), the relative velocity field across the contact area corresponds to a unique center of rotation (discussed below). For rigid bodies this is always true and can be applied for deformable bodies such as soft fingertips since the deformations of the contact area are slow compared to the sliding speed.

A more practical description of the limit surface can be seen in [7]. A two dimensional case is considered, the contact in the sliding plane can be seen in Figure 2.1. A instantaneous motion of a rigid body in the plane can always be described as pure rotation around one point, called the *center of rotation* (COR).

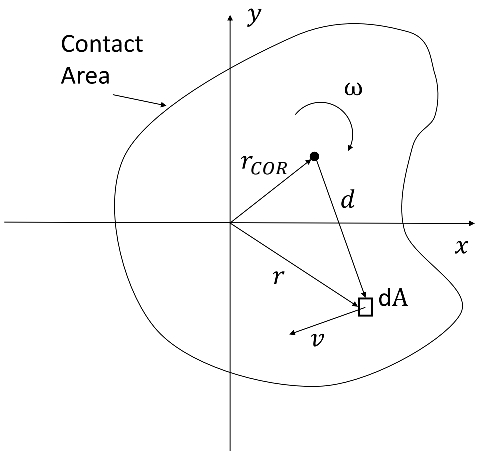

Figure 2.1: Clockwise rotation of the contact around the instantaneous center of rotation (COR) with velocity $\boldsymbol{v}$ at the infinitesimal contact area $\mathrm{d}A$ [7].

Let $\boldsymbol{r}_{COR}$ be the vector from the origin to the instantaneous COR, $\boldsymbol{r} = [x \quad y]^\top$ be the vector from the origin to an element of the contact area and $\boldsymbol{d}(x,y) = [d_x \quad d_y]^\top$ be the vector from the COR to an element of the contact area, i.e. $\boldsymbol{d} = \boldsymbol{r} - \boldsymbol{r}_{COR}$. Through the assumption that the friction is independent of the sliding speed, the velocity can be represented by the unit vector $\hat{\boldsymbol{v}}(x,y) = \boldsymbol{v}(x,y)/|\boldsymbol{v}(x,y)|$. This velocity vector is perpendicular to $\boldsymbol{d}$ since the contact is instantaneously rotating around the COR.

$$\hat{\boldsymbol{v}}(x,y) = \frac{[-d_y \quad d_x]^\top}{|\boldsymbol{d}(x,y)|} \tag{2.1}$$

The local normal force at any point in the contact area is given by $\mathrm{d}f_n = p\mathrm{d}A$, with the local pressure distribution $p(x,y)$ and the infinitesimal area $\mathrm{d}A$ at (x,y). The magnitude of the tangential friction force is calculated with the standard Coulomb friction model $\mathrm{d}f_t = \mu \mathrm{d}f_n$, with $\mu(x,y)$ being the local friction coefficient. The direction of the friction force is always opposed to the velocity at this point, therefore, the local frictional force vector is

$$\mathrm{d}\boldsymbol{f}_t = -\mu p \hat{\boldsymbol{v}} \mathrm{d}A \tag{2.2}$$

and by integrating over the contact area the total frictional force $\boldsymbol{f}_t$ is derived as follows:

$$\boldsymbol{f}_t = \begin{bmatrix} f_x \\ f_y \end{bmatrix} = \int_A \mu p \hat{\boldsymbol{v}}(x,y) \mathrm{d}A. \tag{2.3}$$

The local frictional moment is found by the cross product of the vector $\boldsymbol{r}$ and the local friction force. Since we are in a flat sliding plane, the moment is always perpendicular to the plane and can be considered as scalar. The total torque τ_z is given by the integral

$$\tau_z = -\int_A [\boldsymbol{r} \times \hat{\boldsymbol{v}}] \mu p \mathrm{d}A. \tag{2.4}$$

2.1.1.1 Axisymmetric contacts

Let us assume axisymmetric pressure distribution. Without loss of generality the x-axis can be oriented so that it passes through the COR, with the origin located at the center of the contact region. The vector from the origin to the COR can be written as $\boldsymbol{r}_{COR} = [r_0 \quad 0]^\top$, with r_0 the distance from the origin to the COR. In this case, the frictional force in x-direction f_x is always zero.
By expressing the integrals of (2.3) and (2.4) in polar coordinates we get

$$f_y = -\int_0^{2\pi} \int_0^R \mu(r)p(r) \frac{(r\cos\theta - r_0)r}{\sqrt{r^2 + r_0^2 - 2r_0 r\cos\theta}} \mathrm{d}r\mathrm{d}\theta \tag{2.5}$$

and

$$\tau_z = -\int_0^{2\pi} \int_0^R \mu(r)p(r) \frac{(r - r_0\cos\theta)r^2}{\sqrt{r^2 + r_0^2 - 2r_0 r\cos\theta}} \mathrm{d}r\mathrm{d}\theta \tag{2.6}$$

with R being the radius of the contact area. For these elliptic integrals exist analytic solutions for special cases of pressure distribution.
For a circular contact with uniform pressure distribution Figure 2.2 plots the normalized frictional torque over the normalized frictional force calculated with (2.5) and (2.6) for different distances of the COR to the origin $r_0 \in [0 \quad \infty)$. The frictional force is normalized by the maximal frictional force $f_{y,max} = \mu f_n$ and the frictional torque is normalized by the maximal frictional torque $\tau_{z,max} = 2/3R\mu f_n$. We assume the friction coefficient $\mu(r) = \mu$ is constant.

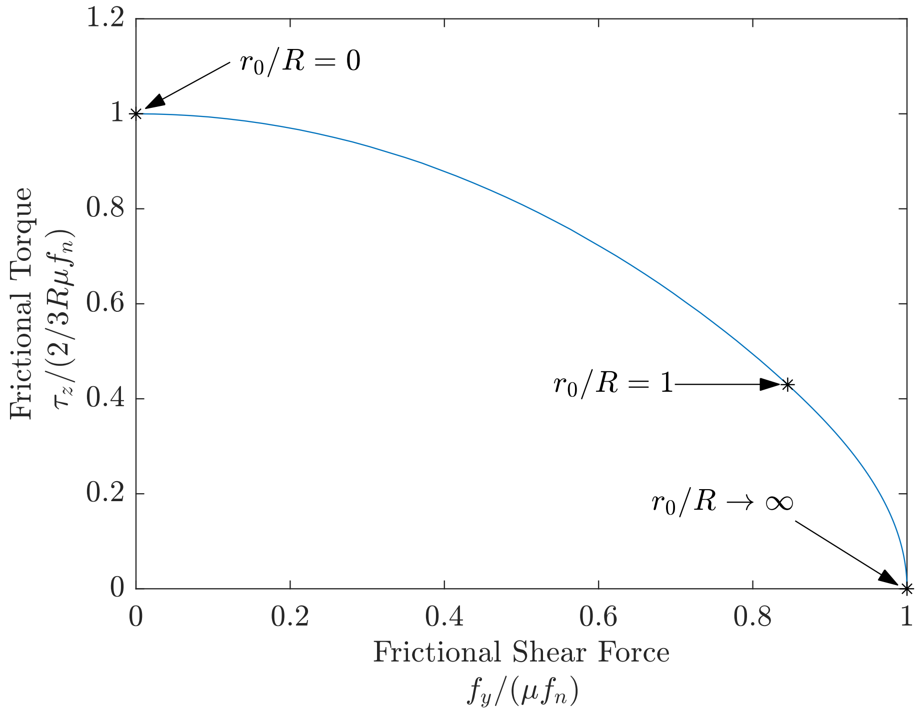

Figure 2.2: Limit curve [7]: normalized frictional force and torque combinations in the force-moment plane for a circular contact with uniform pressure distribution and changing distance of the COR to the origin $r_0 \in [0 \quad \infty)$.

2.1.1.2 Limit curve for different pressure distributions

Different pressure distributions lead to different limit curves since the frictional force and torque calculated with Eq. (2.5) and (2.6) are depended on the local pressure distribution. We consider three cases of pressure distributions, which can be expected with soft fingertips on a robotic or human hand. A Hertzian pressure distribution concentrated at the center [17], an uniform and an annular pressure distribution are investigated. To compare the different pressure distributions, all limit curves get normalized by the maximum frictional force $f_{y,max} = \mu f_n$ and maximal frictional torques, which are shown in Table 2.1 for the different pressure distributions. For the annular pressure distribution, the parameter $s \in (0 \quad 1)$ defines the inner radius of the annulus $s \cdot R$.

Table 2.1: Pressure distribution and maximum torque for Hertzian, uniform and annular pressure distribution [7].

Contact Type	Pressure Distribution	Maximum Torque
Hertzian	$p(r) = \begin{cases} p_0\sqrt{1-\left(\frac{r}{R}\right)^2}, & 0 \leq r \leq R \\ 0, & R < r \end{cases}$ $p_0 = 3f_n/(2\pi R^2)$	$\tau_{z,max} = \frac{3\pi}{16}\mu f_n R$
Uniform	$p(r) = \begin{cases} f_n/(\pi R^2), & 0 \leq r \leq R \\ 0, & R < r \end{cases}$	$\tau_{z,max} = \frac{2}{3}\mu f_n R$
Annular	$p(r) = \begin{cases} 0, & 0 \leq r < sR \\ p_s, & sR \leq r \leq R \\ 0, & R < r \end{cases}$ $p_s = f_n/(\pi R^2(1-s^2)), 0 < s < 1$ $sR =$ inner radius of annulus	$\tau_{z,max} = \frac{2(1-s^3)}{3(1-s^2)}\mu f_n R$

The limit curves of this three cases calculated with (2.5) and (2.6) can be seen in Figure 2.3. We assume that for all three cases the contact radius R is chosen equal and also the normal force f_n is the same each time. The parameter s is set to 0.9. The dotted black line is a normalized ellipse, which is the same of one quarter of the unit circle. This analytic curve lies near the limit curves for all three pressure distributions.

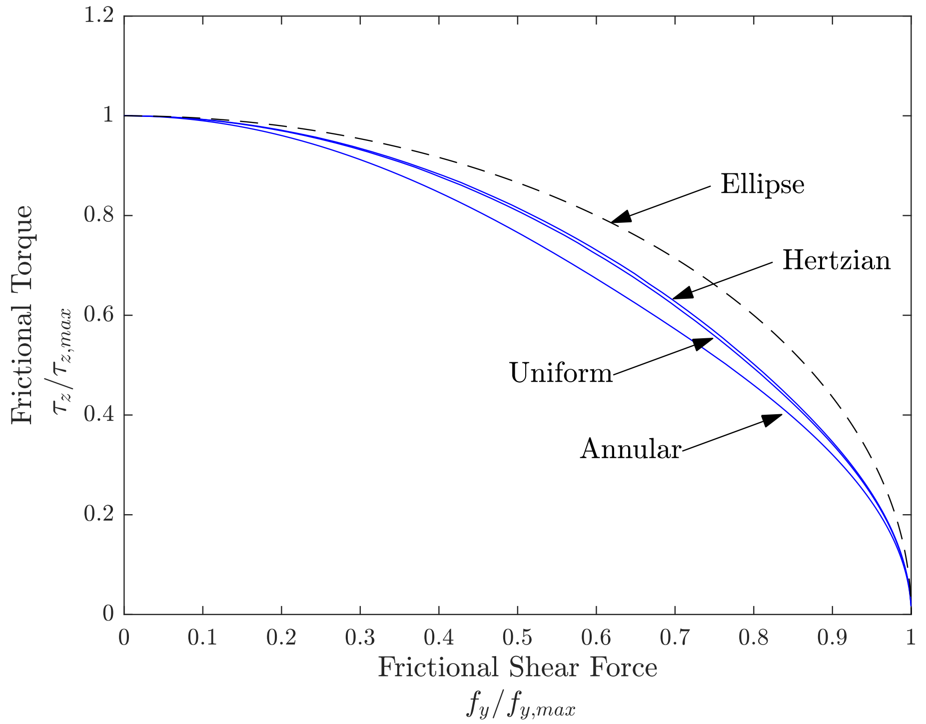

Figure 2.3: Normalized limit curves [7] for Hertzian, uniform and annual pressure distribution for a circular contact and changing distance of the COR to the origin $r_0 \in [0 \quad \infty)$.

The limit curve shows one quarter of the elliptical limit surface. The other three quarters can be calculated by using (2.5) and (2.6) and changing the signs. If the combination of an external tangential force and torque exerted on an object lies inside the corresponding limit surface shown in Figure 2.2, the object will not start sliding. If the point is on the limit surface, a steady sliding will occur and if it is outside the limit surface the contact will slide and accelerate since the applied force and torque exceed the maximal frictional force and torque that the contact can resist. The limit curve or surface explicitly demonstrates the coupling between forces and moments in sliding. The magnitude of the torque required for sliding is decreased as the exerted force increases and vice versa.

The ratio of the translational to the rotational velocity v_t and ω is given by the ratio of the torque τ_z and the tangential frictional force f_y. For the normalized limit surface, the ratio of angular to linear velocity is scaled by the same ratio than the limit surface, $\tau_{z,max}/f_{t,max}$

$$\frac{|v_t|}{\omega} = (\frac{f'_y}{\tau'_z})(\frac{\tau_{z,max}}{f_{t,max}}) \tag{2.7}$$

with the normalized tangential force f'_y and torque τ'_z, the maximal frictional torque $\tau_{z,max}$ and force $f_{t,max}$. The ratio between the translational and rotational velocity is equal to the magnitude of $\boldsymbol{r}_{COR}$. The direction of the translational velocity v_t is always in y-direction, since $f_x = 0$, and opposed to the direction of f_y.

2.1.1.3 Friction force vector

By approximating the limit surface with an ellipsoid Shi et al. show in [4] how the relative velocities and the frictional forces and torques are calculated. As seen in Figure 2.3 the limit surface can be approximated by an ellipsoid in the local contact force space f_x, f_y, τ_z. A mathematical representation of this ellipsoid is given by the following equation:

$$\boldsymbol{f}^\top \boldsymbol{A}\boldsymbol{f} = 1 \tag{2.8}$$

where $\boldsymbol{f} = [f_x, f_y, \tau_z]^\top$ is an arbitrary friction force vector at the contact point and the matrix $\boldsymbol{A} \in \mathbb{R}^{3\times3}$ is a positive definite symmetric matrix that defines the shape of the ellipsoid. The matrix is constructed with the general ellipsoid definition $\boldsymbol{A} = Diag(s_1^{-2}, s_2^{-2}, s_3^{-2})$ where s_1, s_2 and s_3 represent the length of the semi-principal axes. By assuming isotropic dry friction, the maximum tangential force, which can be resisted by the contact, is $f_{t,max} = s_1 = s_2 = \mu f_N$. The maximum moment along the normal direction is $\tau_{z,max} = s_3 = ac\mu f_N$ where a denotes the radius of the contact area and c is a constant. The radius of the contact surface depends on the normal force f_N, thus each normal force has a corresponding contact radius.

While sliding happens, the contact force $\boldsymbol{f}_c$ is on the limit surface and the relative velocity $\Delta\boldsymbol{v}$ is along the direction of the normal to the ellipsoid at that point (Figure 2.4). Therefore, $\boldsymbol{f}_c$ and $\Delta\boldsymbol{v}$ are not always parallel, but they always satisfy $\boldsymbol{f}_c \cdot \Delta\boldsymbol{v} \geq 0$ since friction force can only dissipate energy. For a given friction force $\boldsymbol{f}_c$ and a limit surface we can write the relative velocity $\Delta\boldsymbol{v}$ along the direction of the gradient of the ellipsoid with respect to $\boldsymbol{f}$ at $\boldsymbol{f_c}$:

$$\Delta\boldsymbol{v} = \eta \frac{\partial}{\partial \boldsymbol{f}} \left(\boldsymbol{f}^\top \boldsymbol{A}\boldsymbol{f}\right)\Big|_{\boldsymbol{f}_c} \tag{2.9}$$

where $\eta \in \mathbb{R}$ scales the normal vector to the relative velocity vector. For a given relative velocity, the corresponding friction force is

$$\boldsymbol{f}_c = \frac{1}{\nu}\boldsymbol{B}\eta\Delta\boldsymbol{v} \tag{2.10}$$

where $\boldsymbol{B} = \frac{1}{2}\boldsymbol{A}^{-1}$. Substituting (2.9) in (2.8) and utilizing $(\boldsymbol{A}^{-1})^\top = \boldsymbol{A}^{-1}$ yields

$$\nu = \frac{1}{2}\sqrt{\Delta\boldsymbol{v}^\top \boldsymbol{A}^{-1}\Delta\boldsymbol{v}}. \tag{2.11}$$

Using (2.10) and (2.11) we get the friction force vector as a function of a given relative velocity $\Delta\boldsymbol{v}$

$$\boldsymbol{f}_c = \frac{\boldsymbol{A}^{-1}\Delta\boldsymbol{v}}{\sqrt{\Delta\boldsymbol{v}^\top \boldsymbol{A}^{-1}\Delta\boldsymbol{v}}}. \tag{2.12}$$

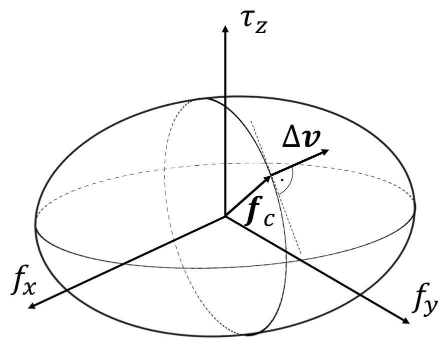

Figure 2.4: Limit surface with a ellipsoidal shape [4]: The tangential friction force is represented by the axes f_x and f_y and the frictional torque is represented by τ_z. The relative velocity $\Delta\boldsymbol{v}$ is along the normal of the ellipsoid at the corresponding friction force vector $\boldsymbol{f}_c$.

2.2 Soft-finger model

The relation between the normal force and the radius of the contact area of two linear elastic objects was first studied by Hertz in [18]. Hertz conducted experiments using a spherical glass lens pressing against a planar glass plate. By using the results of 10 experimental trails, he concluded that the radius of the contact area is proportional to the applied normal force raised to the power of 1/3.

$$a \sim f_n^{\frac{1}{3}} \tag{2.13}$$

where a is the radius of the contact area and f_n is the normal force. The results of the experiments were consistent with the analytical model he derived.

An alternative theory for modeling soft finger contacts is proposed in [8].
For incompressible nonlinear elastic materials, the 3-D constitutive relation is given by following equations [19]

$$\epsilon_{ij} = \left(\frac{\sigma_e}{k_s}\right)^n \frac{\partial}{\partial \sigma_{ij}} \tag{2.14}$$

$$\sigma_{ij} = \sigma_e \frac{\partial}{\partial \epsilon_{ij}} \left(\frac{\sigma_e}{k_s}\right)^n \tag{2.15}$$

where σ_{ij} and ϵ_{ij} are the stress and strain components in i and j directions. σ_e is the Von Mises stress, k_s is a constant with stress units and n is the stress exponent for nonlinear elastic materials ($n \leq 1$).
The Von Mises stress is

$$\sigma_e = \sqrt{\frac{3}{2} S_{ij} S_{ij}} = \sqrt{\frac{3}{2}(\sigma_{ij} - \frac{1}{3}\sigma_{kk}\delta_{ij})(\sigma_{ij} - \frac{1}{3}\sigma_{kk}\delta_{ij})} \tag{2.16}$$

where S_{ij} are the components of the stress deviatior tensor and $\frac{1}{3}\sigma_{kk}\delta_{ij}$ is the hydrostatic stress tensor. The strain components are given by

$$\epsilon_{ij} = \frac{1}{2}\left(\frac{\partial u_i}{\partial x_j} + \frac{\partial u_j}{\partial x_i}\right) \tag{2.17}$$

where u_i is the infinitesimal displacement and $\frac{\partial u_j}{\partial x_i}$ is the derivative of u_i with respect to the jth orthogonal coordinate in the Cartesian coordinates. The stress equilibrium requires following condition

$$\frac{\partial \sigma_{ij}}{\partial x_j} = 0. \tag{2.18}$$

Considering a nonlinear elastic sphere, shown in Figure 2.5, with the radius R_0 being pushed onto a rigid plane. In the cylindrical polar coordinates the boundary conditions at the surface are

$$\sigma_t = \sigma_n = 0 \qquad \text{for } r > a \text{ (no contact)} \tag{2.19}$$

$$u = u(r) = d - \left(R_0 - \sqrt{R_0^2 - r^2}\right) \qquad \text{for } r < a \text{ (in contact)} \tag{2.20}$$

where σ_t and σ_n are the tangential and normal stresses, respectively, $u(r)$ is the displacement of the spherical surface in the contact zone, d is the displacement in the contact zone at $r = 0$ and a is the radius of the contact area, as shown in Figure 2.5.

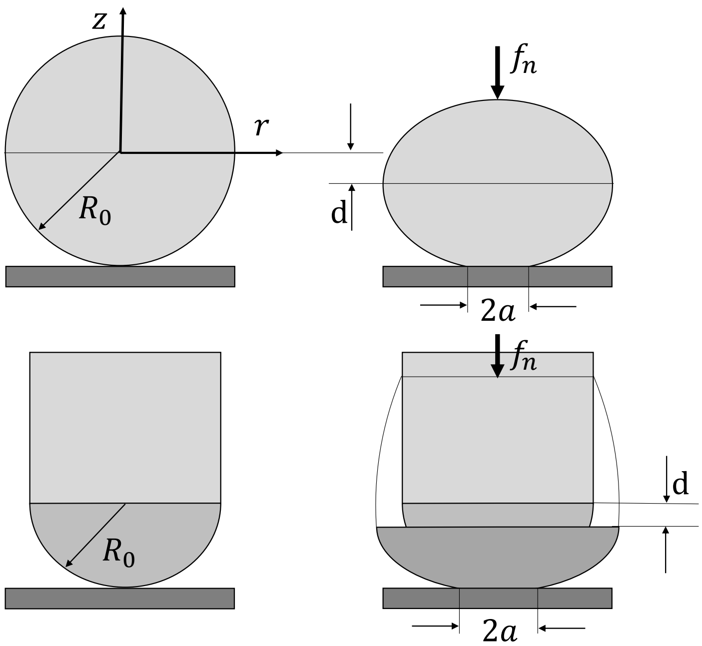

Figure 2.5: A model of a nonlinear elastic sphere in contact with a surface [19], pushed by a normal force f_n (top) and a model of a hemispherical soft finger being pushed on a rigid plane (bottom). In both models the contact area is assumed circular.

The force balance for the circular contact area requires that

$$f_n = \int_0^{2\pi} \int_0^a \sigma_{zz} r \mathrm{d}r \mathrm{d}\theta = \pi \int_0^a \sigma_{zz} \mathrm{d}(r^2) \tag{2.21}$$

with the stress component σ_{zz} normal to the contact surface in polar coordinates. By defining the following dimensionless variables

$$\tilde{r} = \frac{r}{a}, \quad \tilde{z} = \frac{z}{a}, \quad \tilde{x} = \frac{x}{a}, \quad \tilde{u}_i = \frac{u_i R_0}{a^2} \tag{2.22}$$

where u_i is given by (2.20) and substituting $\tilde{x}$ and $\tilde{u}$ into (2.17), we obtain

$$\epsilon_{ij} = \frac{a}{R_0} \tilde{\epsilon}_{ij} \tag{2.23}$$

where $\tilde{\epsilon}_{ij} = \frac{1}{2}\left(\frac{\partial \tilde{u}_i}{\partial \tilde{x}_j} + \frac{\partial \tilde{u}_j}{\partial \tilde{x}_i}\right)$. From Equation (2.14), after the substitution of ϵ_{ij} in (2.23) and σ_e in (2.16), we get

$$\sigma_{ij} \sim \left(\frac{a}{R_0}\right)^{\frac{1}{n}} \tilde{\sigma}_{ij} \tag{2.24}$$

Substitute Eq. (2.22) and (2.24) into (2.21) leads to

$$\frac{f_n}{\pi a^2} = \int_0^a \sigma_{zz} \mathrm{d}\left(\frac{r^2}{a^2}\right) \sim \left(\frac{a}{R_0}\right)^{\frac{1}{n}} \int_0^1 \tilde{\sigma}_{zz} \mathrm{d}\left(\tilde{r}^2\right). \tag{2.25}$$

The integration of (2.25) is dimensionless. By combining all constant terms, we obtain

$$f_n = c_1 a^{\frac{1}{n}+2} \tag{2.26}$$

or

$$a = c f_n^{\frac{n}{2n+1}} = c f_n^{\gamma} \tag{2.27}$$

with the exponent of the normal force $\gamma = \frac{n}{2n+1}$ and the constant $c = 1/c_1$, which depends on the size and curvature of the fingertips and its material properties. The parameter n is between 0 and 1 [19], thus the exponent in Equation (2.27) is

$$0 \leq \gamma \leq \frac{1}{3}. \tag{2.28}$$

If $\gamma = 0$ we have the case of the ideal soft finger. The radius of the contact area is constant and independent of the normal force. For $\gamma = 1/3$ we have the Hertzian contact model shown above.

2.3 Nonlinear adaptive control

For some important classes of nonlinear control problems, adaptive control has been developed [9]. This nonlinear control problems usually satisfy following assumptions:

1. The full state is measurable.
2. Nonlinearities can be canceled stably with the control input if the parameters are known.
3. The nonlinear plant dynamics can be parametrized linearly.

We consider n^{th}-order *Single-Input and Single-Output* (SISO) systems

$$y^{(n)} + \sum_{i=1}^{n} \alpha_i f_i(\boldsymbol{x}, t) = bu \tag{2.29}$$

with the state vector $\boldsymbol{x} = [y \quad \dot{y} \quad \dots \quad y^{(n-1)}]^\top$, unknown constants α_i and b and known nonlinear functions of the state and time f_i. With the assumption, that the state is measurable and the sign of b is know, Equation (2.29) can be rewritten as

$$hy^{(n)} + \sum_{i=1}^{n} a_i f_i(\boldsymbol{x}, t) = u \tag{2.30}$$

where $h = 1/b$ and $a_i = \alpha_i/b$.
Let us define a combined error

$$s = e^{(n-1)} + \lambda_{n-2} e^{(n-2)} + \ldots + \lambda_0 e = \Delta(p)e \tag{2.31}$$

with the output tracking error e and a stable polynomial $\Delta(p) = p^{(n-1)} + \lambda_{n-2} p^{(n-2)} + \ldots + \lambda_0$ in the Laplace variable p. The combined error s can be rewritten as

$$s = y^{(n-1)} - y_r^{(n-1)} \tag{2.32}$$

where $y_r^{(n-1)}$ is defined as

$$y_r^{(n-1)} = y_d^{(n-1)} - \lambda_{n-2} e^{(n-2)} - \ldots - \lambda_0 e \tag{2.33}$$

where y_d is the desired output given by a reference model.
Consider the control law

$$u = hy_r^{(n)} - ks + \sum_{i=1}^{n} a_i f_i(\boldsymbol{x}, t) \tag{2.34}$$

with the constant k, which has the same sign as h and $y_r^{(n)}$, the derivative of $y_r^{(n-1)}$

$$y_r^{(n)} = y_d^{(n)} - \lambda_{n1} e^{(n)} - \ldots - \lambda_0 \dot{e}. \tag{2.35}$$

It has to be noted that $y_r^{(n)}$ is a reference value of $y^{(n)}$, which is obtained by modifying $y_d^{(n)}$ according to the tracking error. If the parameters h and a_i are known the choice of this control law leads to the tracking error dynamics by substituting (2.34) in (2.30):

$$h\dot{s} + ks = 0. \tag{2.36}$$

This gives an exponential convergence of s, and therefore guarantees a convergence of e.

To get an adaptive control, the constants h and a_i of the control law (2.34) get replaced by their estimates $\hat{h}$ and $\hat{a}_i$

$$u = \hat{h}y^{(n)} - ks + \sum_{i=1}^{n} \hat{a}_i f_i(\boldsymbol{x}, t). \tag{2.37}$$

The dynamics of the tracking error of this control law is

$$h\,\dot{s} + k\,s = \tilde{h}\,y_r^{(n)} + \sum_{i=1}^{n} \tilde{a}_i f_i(\boldsymbol{x}, t) \tag{2.38}$$

where $\tilde{h} = \hat{h} - h$ and $\tilde{a}_i = \hat{a}_i - a_i$ for $i = 1 \ldots n$. The tracking error can be rewritten with the Laplace variable p to

$$s = \frac{1/h}{p + (k/h)}[\tilde{h}\,y_r^{(n)} + \sum_{i=1}^{n} \tilde{a}_i f_i(\boldsymbol{x}, t)]. \tag{2.39}$$

Since the transfer function is strictly positive real, the following control law is chosen by employing Lemma 8.1 of [9]:

$$\dot{\hat{h}} = -\gamma\; sgn(h)\; s\; y_r^{(n)} \tag{2.40}$$

$$\dot{\hat{a}}_i = -\gamma\; sgn(h)\; s\; f_i. \tag{2.41}$$

2.4 Prescribed error bounds

A control structure, which is independent from the model, and therefore is suitable for any nonlinearities, is presented in [10]. Karayiannidis et al. show a guaranteed prescribed transient and steady state behavior for the position and the velocity tracking error of a robot joint without compensating for the robot dynamics.

To achieve prescribed performance, each element e_i, $i = 1, \ldots, n$ of a generic tracking error $\boldsymbol{e} \in \mathbb{R}^n$ has to satisfy $\forall t \geq 0$:

$$\underline{b}_i(t) < e_i < \overline{b}_i(t) \tag{2.42}$$

where $\underline{b}_i(t), \overline{b}_i(t) : \mathbb{R}_{\geq 0} \to \mathbb{R}_{>0}$ are the continuous and bounded performance bounds. Utilizing strictly positive, decreasing and bounded performance functions $\rho_i(t)$ and constant overshoot indices $M_i \in (0, 1]$, leads directly to the desired transient and steady state bounds in e_i. By denoting $e_{0i} = e_i(0)$, the performance bounds of Eq. (2.42) are given by:

$$\underline{b}_i(t) = -M_i \rho_i(t), \quad \overline{b}_i(t) = \rho_i(t) \qquad \text{for} \quad e_{0i} \geq 0 \tag{2.43}$$

$$\underline{b}_i(t) = -\rho_i(t), \qquad \overline{b}_i(t) = M_i \rho_i(t) \quad \text{for} \quad e_{0i} \leq 0 \tag{2.44}$$

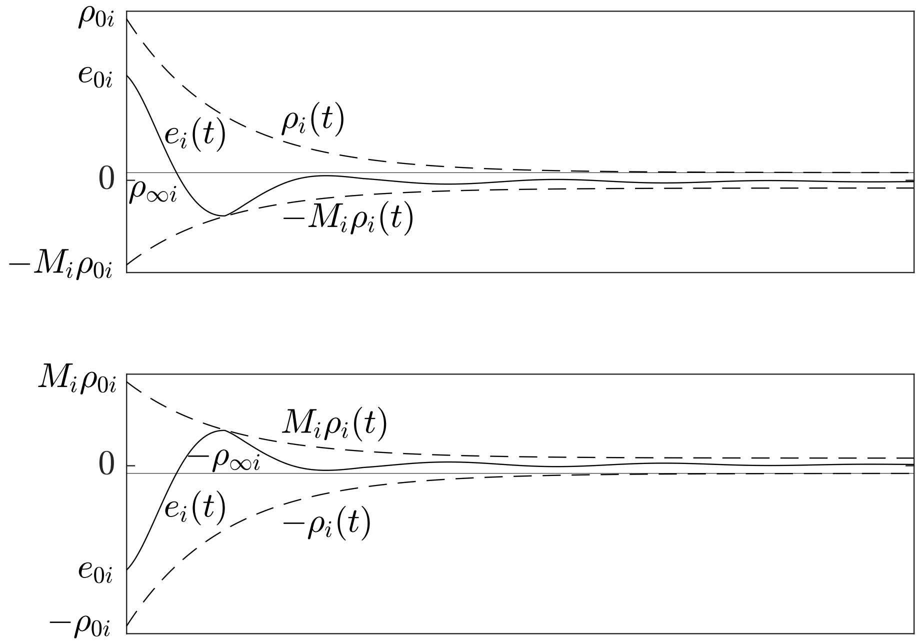

Figure 2.6: Performance bounds [10]: $e_i(t)$ denotes the tracking error, $\rho_i(t)$ is the performance function. e_{i0} and ρ_{0i} are the corresponding values for $t = 0$. M_i is a constant which scales the performance function and $\rho_{\infty i}$ is the maximal allowable size of e_i at the steady state.

For each e_i, one of the performance bounds of (2.43) or (2.44) belonging to e_{0i} is employed. If $e_{0i} = 0$ either (2.43) or (2.44) can be used. Figure 2.6 shows an error element evolution with prescribed performance for an exponentially decaying performance function defined as follows:

$$\rho_i(t) = (\rho_{0i} - \rho_{\infty i}) \exp(-l_i t) + \rho_{\infty i} \tag{2.45}$$

where ρ_{0i}, l_i and $\rho_{\infty i}$ are strictly positive constants and $\rho_{0i} = \rho_i(0)$ is chosen such that $\rho_{0i} > |e_{0i}|$. The maximum allowable size of e_i at the steady state is denoted by $\rho_{\infty i} = \lim_{t\to+\infty} \rho_i(t)$. The constant l_i influences the decreasing rate of $\rho_i(t)$, which is a lower bound on the required speed of convergence of e_i. The maximal allowable overshoot is less than $M_i\rho_{0i}$.
The normalized tracking error is defined as $\hat{e}_i \triangleq \frac{e_i}{\rho_i(t)}$ and with $\rho_{0i} > |e_{0i}|$ the prescribed performance inequalities can be written as $\hat{e}_i \in \Omega_i$. The open sets Ω_i, $i = 1, \ldots, n$ are defined as follows:

$$\Omega_i = \{\hat{e}_i \in \mathbb{R} : -M_i < \hat{e}_i < 1\} \text{ in case of } \quad e_{0i} \geq 0 \tag{2.46}$$

$$\Omega_i = \{\hat{e}_i \in \mathbb{R} : -1 < \hat{e}_i < M_i\} \text{ in case of } \quad e_{0i} \leq 0 \tag{2.47}$$

An error transformation proposed in [20] and modified in [21] is used to introduce prescribed performance. We define the components ξ_i of the transformed error $\boldsymbol{\xi} \in \mathbb{R}^n$:

$$\xi_i = T_i(\hat{e}_i) \tag{2.48}$$

where $T_i(\cdot)$, $i = 1, \ldots, n$ are the transformation functions which are strictly increasing, smooth functions defining bijective mappings:

$$T_i : \Omega_i \to (-\infty, \infty) \tag{2.49}$$

with $T_i(0) = 0$.
By the differentiation of (2.48) with respect of the time we get:

$$\dot{\xi}_i = J_i \left[\dot{e}_i + \alpha_i(t) e_i\right] \tag{2.50}$$

where J_i, denotes the normalized slope of $T_i(\hat{e}_i)$, and $\alpha_i(t)$ are given by:

$$J_i \triangleq \frac{\partial T_i}{\partial \hat{e}_i} \frac{1}{\rho_i(t)} > 0 \tag{2.51}$$

$$\alpha_i(t) \triangleq -\frac{\dot{\rho}(t)}{\rho_i(t)} \geq 0 \tag{2.52}$$

According to (2.49), a candidate error transformation is defined as:

$$T_i(\hat{e}_i) = \ln\left[\frac{M_i + \hat{e}_i}{M_i(1 - \hat{e}_i)}\right] \quad \text{in case of} \quad e_{0i} \geq 0 \tag{2.53}$$

$$T_i(\hat{e}_i) = \ln\left[\frac{M_i(1 + \hat{e}_i)}{M_i - \hat{e}_i}\right] \quad \text{in case of} \quad e_{0i} \leq 0 \tag{2.54}$$

Equations (2.53) and (2.54) are plotted in Fig. 2.7.

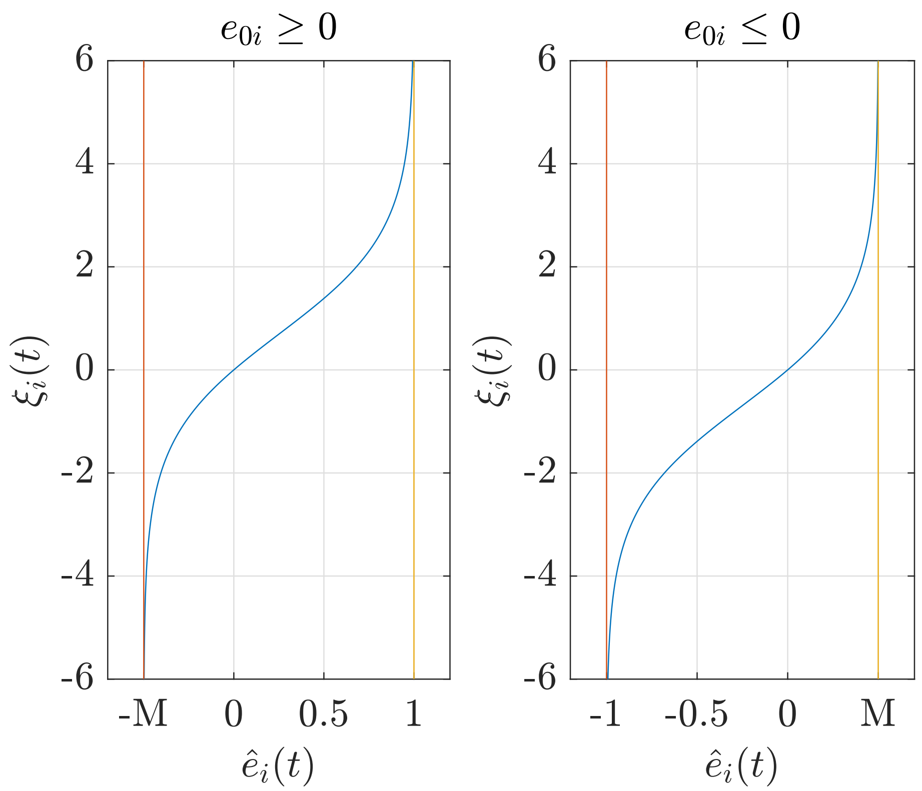

Figure 2.7: Error transformation with natural logarithm [10]. Illustration of (2.53) and (2.54).

By designing prescribed performance controller as proposed in [22], the tracking error evolves strictly within the prescribed performance bounds of (2.42).

3

Modeling and Problem Description

In this thesis we consider specific in-hand manipulation via extrinsic dexterity where an object is grasped by a one degree of freedom parallel jaw gripper and the gravity of the grasped object is used to regulate its orientation (Figure 3.1).

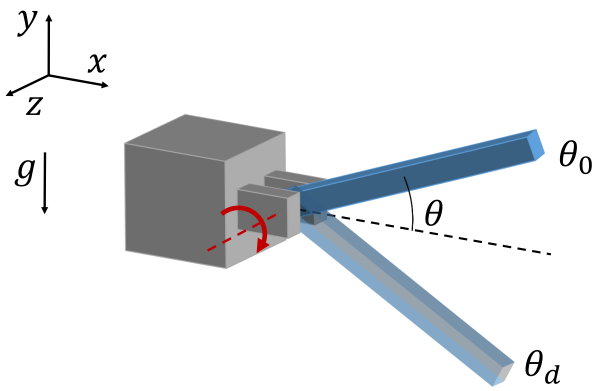

Figure 3.1: Modeling of the in-hand manipulation task: the blue object is grasped by the gripper and rotates around the z-axis. The orientation of the object is denoted by θ, θ_0 is the initial angular position, θ_d is the desired end position and g denotes the gravitational acceleration.

The problem can be divided in two parts. First, a suitable model has to be derived to simulate the contact between the fingertips and the object. Second, a controller has to be designed to control the actual orientation of the grasped object to a desired orientation.

3.1 Modeling

The contact model describes the friction between the object and the fingertips and the deformation of them. The generalized friction force consist of a frictional force and torque that are exploited in order to perform the manipulation task. The standard Coulomb model can handle both of them only separately, independent of each other. However, in [13] and [14] it is shown that they have a dependency. One way to model the contact with depended frictional force and torque is the concept of the limit surface described in Section 2.1.

Figure 3.2 shows the conceptual model of the dependency between the contact model and the model of the object. With the normal force of the gripper and the gravitational force and torque of the object, the contact model calculates the frictional force and torque which is applied at the contact area.

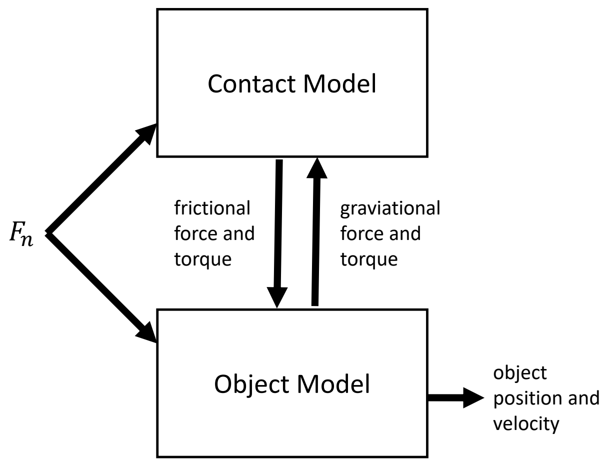

Figure 3.2: Conceptual visualization of the contact model and its dependency to the grasped object

An object grasped by a parallel jaw gripper can be seen in Figure 3.3. It is assumed that the pivoting task is a planar problem.

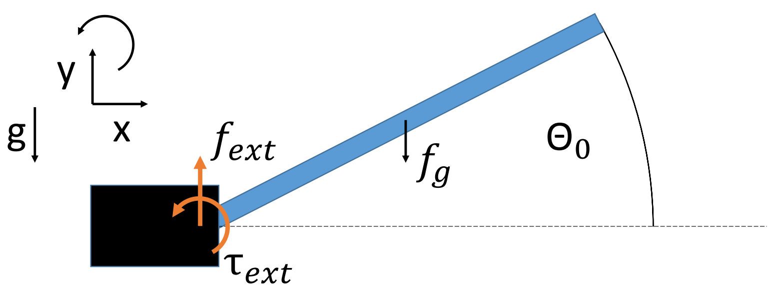

Figure 3.3: Modeling of the pivoting task (left). g is the gravitational acceleration and θ is the orientation of the object. On the right side the gripper is replaced with the friction force and torque, which is applied from the gripper. The gravitational force mg is exerted at the *center of mass* (COM) of the object, which has the distance l_{Center} from the grasping point.

The blue bar is the object, which is grasped at the left side from the gripper (black). On the right side, the gripper is replaced with the frictional force f_t and torque τ_f, which results from the normal force applied from one finger. Since the assumption is made that the grasp is symmetric, the normal forces exerted by each finger on the object are equal and therefore, the resulting frictional force and torque is $2f_t$ and $2\tau_f$, respectively. *The center of mass* (COM) of the object has a distance of l_{Center} from the grasping point. The rotational dynamics of the object are given by

$$I\ddot{\theta} = \tau_g + 2\tau_f \tag{3.1}$$

where I is the moment of inertia of the object around the axis of rotation and $\ddot{\theta}$ is the angular acceleration of the object. The gravitational torque is denoted by $\tau_g = f_g l_{center} \cos(\theta)$, where $f_g = -mg$ is the gravitational force, m is the mass of the object, g is the acceleration of gravity and θ is the angular orientation of the object. The combined rotational and translational dynamics of the object are given by

$$\boldsymbol{M}\ddot{\boldsymbol{q}} = \boldsymbol{g} + 2\boldsymbol{f_c} \tag{3.2}$$

where $\boldsymbol{M} = Diag(m, m, I)$ is the mass matrix of the object, $\ddot{\boldsymbol{q}} = [a_x, a_y, \ddot{\theta}]^\top$ is the acceleration vector of the object, $\boldsymbol{f_c}$ is the friction force/torque set of the fingers and $\boldsymbol{g} = [0 \quad -mg \quad -mgl_{Center}\cos\theta]^\top$ is the gravitational force and torque applied to the object.

3.1.1 Limit surface

The robotic fingertip contact model is modeled as soft finger contact. The soft finger contact model assumes that the finger can exert both friction force tangential to the contact surface and torsional friction around the direction normal to the contact surface. The limit surface is the boundary if slippage happens or not and can be approximated by the ellipsoid [4]

$$\boldsymbol{f}^\top \boldsymbol{A}\boldsymbol{f} = 1 \tag{3.3}$$

with

$$\boldsymbol{f} = [f_x, f_y, \tau_z]^\top \tag{3.4}$$

where (f_x, f_y) are the tangential friction force components and τ_z is the torsional friction around the normal. By the assumption of isotropic friction the matrix $\boldsymbol{A} \in \mathbb{R}^{3\times3}$ becomes a diagonal matrix, whose elements are the maximum friction force and moment

$$\boldsymbol{A} = diag(f_{t,max}^{-2}, f_{t,max}^{-2}, \tau_{z,max}^{-2}) \tag{3.5}$$

The tangential force can be modeled as Coulomb friction

$$f_{t,max} = \mu \cdot f_n \tag{3.6}$$

where μ is the friction coefficient and f_n is the normal force applied from the gripper. The maximum torsional friction $\tau_{z,max}$ is given by the equation [6]

$$\tau_{z,max} = a\beta\mu f_n \tag{3.7}$$

where a is the radius of the contact surface and β is a constant depending on the local pressure distribution. In this case we assume Hertzian pressure distribution, which leads to $\beta = 0.589$ [7]. From Section 2.2 we get

$$a = cf_n^{\gamma} \tag{3.8}$$

where c is a constant, which depends on the size and curvature of the fingertips and its material properties, and γ is a constant value between 0 and 1/3 depending on the material of the fingertips [8]. By substituting Eq. (3.8) in (3.7) we get

$$\tau_{z,max} = \mu_{tors} \cdot f_n^{1+\gamma} \tag{3.9}$$

where the torsional friction coefficient $\mu_{tors} = c\beta\mu$.
Since there is no force in x-direction, f_x is zero and the limit surface is a 2-dimensional ellipse. To normalize the ellipse, each point (f, τ) is scaled such that $(f', \tau') = (f/f_{t,max}, \tau/\tau_{z,max})$. The normalized ellipse is simply a circle, which is scaled with the normal force applied from the gripper. Figure 3.4 shows the normalized ellipse. For a given normalized external force f'_g and torque τ'_g, which correspond to the gravitational force and torque, the resulting normalized frictional force and torque is f'_t and τ'_f, respectively.

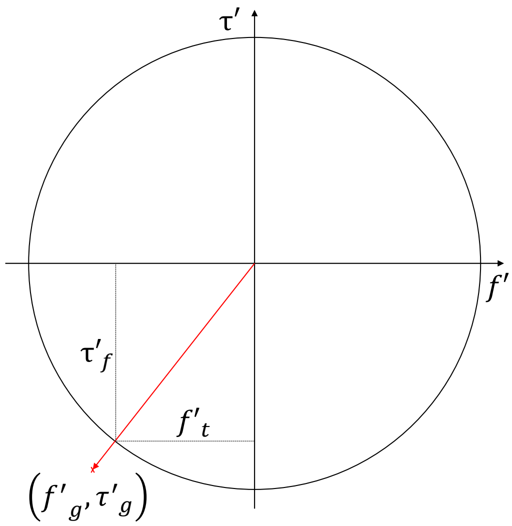

Figure 3.4: Limit surface: normalized ellipse (f', τ') with the corresponding normalized frictional force and torque f'_t and τ'_f for a given external force and torque f'_g and τ'_g

This leads to the following equations to calculate the normalized frictional force f'_t

and torque τ_t':

$$f_t' = \begin{cases} \sin(\arctan(f_g'/\tau_g') - \pi), & (v_t \neq 0 \vee |f_g| \geq 2f_t) \wedge (f_g' < 0,\ \tau_g' < 0) \\ \sin(\arctan(f_g'/\tau_g')), & (v_t \neq 0 \vee |f_g| \geq 2f_t) \wedge \neg(f_g' < 0,\ \tau_g' < 0) \\ -f_g', & (v_t = 0 \wedge |f_g| < 2f_t) \end{cases} \tag{3.10}$$

$$\tau_f' = \begin{cases} \cos(\arctan(f_g'/\tau_g') - \pi), & (\dot{\theta} \neq 0 \vee |\tau_g| \geq 2|\tau_f|) \wedge (f_g' < 0,\ \tau_g' < 0) \\ \cos(\arctan(f_g'/\tau_g')), & (\dot{\theta} \neq 0 \vee |\tau_g| \geq 2|\tau_f|) \wedge \neg(f_g' < 0,\ \tau_g' < 0) \\ -\tau_g', & (\dot{\theta} = 0 \wedge |\tau_g| < 2|\tau_f|) \end{cases} \tag{3.11}$$

where

$$f_g' = f_g/2f_{t,max} \tag{3.12}$$

$$\tau_g' = \tau_g/2\tau_{z,max} \tag{3.13}$$

and $\dot{\theta}$ and v_t are the angular and tangential velocities. By multiplying the normalized frictional force f_t' and torque τ_t' with the maximal tangential friction $f_{t,max}$ and maximum torsional friction $\tau_{z,max}$ respectively we get the frictional force f_t and torque τ_t

$$f_t = f_t' f_{t,max} \tag{3.14}$$

$$\tau_f = \tau_f' \tau_{z,max}. \tag{3.15}$$

The relation between the angular and translational velocity v_y and $\dot{\theta}$ is given by the equation

$$\frac{|v_t|}{\dot{\theta}} = \lambda \frac{f_y'}{\tau_g'} \tag{3.16}$$

with

$$\lambda = \frac{\tau_{z,max}}{f_{t,max}} \tag{3.17}$$

with this relationship it is enough to obtain either the rotational or the translational sliding dynamics and calculate the corresponding translational or rotational velocity with Equation (3.16).

3.1.2 Rotational model

The rotational model utilizes dynamics for the rotation and calculates the translational velocity with a dependency to the rotational velocity in most of the pivoting tasks. The equations derived in Section 3.1.1 are used to deduce the dynamics of the grasped object.

Figure 3.5 shows the limit surface. In the blue area (A) the rotational dynamics are considered and the translational velocity is calculated using (3.16). In the green area (B), both the rotational and translational dynamics are considered. Thus, if the magnitude of the induced torque is bigger than the magnitude of the normalized gravitational force, the relation between the rotational and translational velocities is considered and if the magnitude of the normalized gravitational force is bigger than the magnitude of the induced torque, the object dynamics are used for the rotational and translational dynamics. We have differentiated the modeling depending on the region, because the relation between the translational and rotational velocity (3.16) is not valid if the gravitational torque is zero. A gravitational torque equals to zero would lead to an infinite translational velocity.

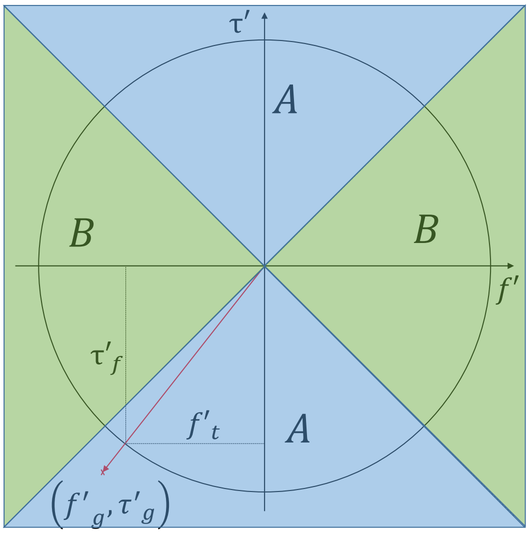

Figure 3.5: Limit surface: normalized ellipse (f', τ') with two regions A (blue) and B (green). In the blue area the normalized torque is bigger than the normalized force and in the green area it is vice versa.

For region A, the rotational dynamics of the configuration seen in Figure 3.3 are given by

$$I\ddot{\theta} = \begin{cases} \tau_g - sign(\tau_g)2|\tau_f|, & \dot{\theta} = 0 \\ \tau_g - sign(\dot{\theta})2|\tau_f|, & \dot{\theta} \neq 0 \end{cases} \tag{3.18}$$

By inserting τ_f and resolving the equation to $\ddot{\theta}$, (3.18) can be rewritten as

$$\ddot{\theta} = \begin{cases} \frac{\tau_g - sign(\tau_g)2|\cos(\arctan(f'_g/\tau'_g))|\cdot\tau_{z,max}}{I}, & (\dot{\theta} = 0 \wedge |\tau_g| > 2|\tau_f|) \\ 0, & (\dot{\theta} = 0 \wedge |\tau_g| \leq 2|\tau_f|) \\ \frac{\tau_g - sign(\dot{\theta})2|\cos(\arctan(f'_g/\tau'_g))|\cdot\tau_{z,max}}{I}, & \dot{\theta} \neq 0. \end{cases} \tag{3.19}$$

The translational velocity can be obtained from Eq. (3.16). The direction of the translational velocity is always in negative y-direction since the only external force is the gravitational force, which exerts in this direction.

$$v_y = -|\lambda \frac{f'_y}{\tau'_g}\dot{\theta}| \tag{3.20}$$

where v_y denotes the velocity in y-direction.
For region B, the translational dynamics are given by

$$ma_y = f_g + 2f_t \tag{3.21}$$

where a_y is the translational acceleration in y-direction. By inserting f_t in (3.21) and resolving the equation for a_y we get

$$a_y = \begin{cases} \frac{f_g + 2\sin(\arctan(f'_g/\tau'_g)-\pi)\cdot f_{t,max}}{m}, & (v_t \neq 0 \lor |f_g| \geq 2f_t) \land (f'_g < 0,\ \tau'_g < 0) \\ \frac{f_g + 2\sin(\arctan(f'_g/\tau'_g))\cdot f_{t,max}}{m}, & (v_t \neq 0 \lor |f_g| \geq 2f_t) \land \neg(f'_g < 0,\ \tau'_g < 0) \\ 0, & (v_t = 0 \land |f_g| < 2f_t). \end{cases} \tag{3.22}$$

The rotational dynamics are given by Eq. (3.18) and (3.19). It has to be noted that the Region A and B have been chosen the same size. However, the border between both regions can be set different. Since the focus for our model is on the rotational dynamics where the gravitational torque is much bigger than the gravitational force, we stay most of the time in region A and the borderline to region B can be seen as insignificant.

3.1.3 Combined model

The rotational model derived before calculates only the rotational dynamics if the normalized gravitational torque is bigger than the normalized gravitational force, which we expect for most of the pivoting tasks. The translational velocity is computed with the help of the ratio of the translational and rotational velocities. This heuristic can not cover the real translational dynamics since no translational accelerations is considered. To cover both the rotational and the translational dynamics of the object, a combined model, which is based on the theory shown in Section 2.1.1.3, is derived. The limit surface constructed in Section 3.1.1 is still used.

To recap the combined rotational and translational object dynamics (3.2) are defined as

$$\boldsymbol{M}\ddot{\boldsymbol{q}} = 2\boldsymbol{f_c} + \boldsymbol{g}.$$

The theory shown in Section 2.1.1.3 is used to calculate the frictional force and torque $\boldsymbol{f_c}$. We define the relative velocity vector

$$\Delta\boldsymbol{v} = -\dot{\boldsymbol{q}} \tag{3.23}$$

where $\dot{\boldsymbol{q}}$ is the velocity vector of the object. The friction force vector is given by

$$\boldsymbol{f}_c = \begin{cases} \frac{\boldsymbol{A}^{-1}\Delta\boldsymbol{v}}{\sqrt{\Delta\boldsymbol{v}^\top\boldsymbol{A}^{-1}\Delta\boldsymbol{v}}}, & \Delta\boldsymbol{v} \neq 0 \\ -\frac{1}{2}\boldsymbol{g}, & \sqrt{f'^2_g + \tau'^2_g} \leq 1 \ and\ \Delta\boldsymbol{v} = 0 \\ \frac{\boldsymbol{A}^{-1}\boldsymbol{r}_{ft}}{\sqrt{\boldsymbol{r}_{ft}^\top\boldsymbol{A}^{-1}\boldsymbol{r}_{ft}}}, & \sqrt{f'^2_g + \tau'^2_g} > 1 \ and\ \Delta\boldsymbol{v} = 0 \end{cases} \tag{3.24}$$

where f'_g and τ'_g are the normalized frictional force and torque respectively. It has to be noted that in the third case of Eq. (3.24) the relative velocity $\Delta\boldsymbol{v}$ is substituted by the force and torque ratio $\boldsymbol{r}_{ft}$, which corresponds to the velocity ratio of Eq. (3.16)

$$\boldsymbol{r}_{ft} = [0 \quad |\lambda \frac{f'_y}{\tau'_g}| \quad - sign(\tau_g)]^\top \tag{3.25}$$

where $\lambda = \tau_{z,max}/f_{t,max}$. Since the relative velocity vector is always opposed to the velocity of the object and the velocity in y-direction of the object is always smaller or equal to zero, the second component of $\boldsymbol{r}_{ft}$ is always positive. The third component is opposed to the gravitational torque. By inserting (3.24) in (3.2) we obtain the acceleration of the object:

$$\ddot{\boldsymbol{q}} = \begin{cases} \boldsymbol{M}^{-1}(2\frac{\boldsymbol{A}^{-1}\Delta\boldsymbol{v}}{\sqrt{\Delta\boldsymbol{v}^\top\boldsymbol{A}^{-1}\Delta\boldsymbol{v}}} + \boldsymbol{g}), & \Delta\boldsymbol{v} \neq 0 \\ 0, & \sqrt{{f'_g}^2 + {\tau'_g}^2} \leq 1 \ and \ \Delta\boldsymbol{v} = 0. \\ \boldsymbol{M}^{-1}(2\frac{\boldsymbol{A}^{-1}\boldsymbol{r}_{ft}}{\sqrt{\boldsymbol{r}_{ft}^\top\boldsymbol{A}^{-1}\boldsymbol{r}_{ft}}} + \boldsymbol{g}), & \sqrt{{f'_g}^2 + {\tau'_g}^2} > 1 \ and \ \Delta\boldsymbol{v} = 0 \end{cases} \tag{3.26}$$

It is notable that the combined model covers the translational dynamics in x- and y-direction and the rotational dynamics. However, since we have no forces acting in x-direction, the acceleration in x-direction is always zero and the problem could be easily adapted to a two dimensional problem by cutting the first row of all vectors and matrices.

3.2 Validation and comparison of the models

To validate the derived contact models in Section 3.1.2 and 3.1.3 the models are built in Matlab and Simulink. An ode3 solver with a step size of 10^{-4} is used. Table 3.1 shows the parameter of the grasped object. The object parameters are gathered from [6]. The parameter γ, which depends on the material of the fingertips, is set to 0.3.

Table 3.1: Parameter of the grasped object.

m [g]	48.5
l_{center} [cm]	12.22
I [Kg $\cdot$ cm^2]	10.64
μ	0.47
μ_{tors}	0.643 $\cdot 10^{-3}$

3.2.1 Constant grasping force

The grasped object has an initial orientation of 27°, which corresponds to Fig. 3.3. A constant grasping force of 20 N is applied to the object.

The normalized limit surface can be seen in Figure 3.6. The red point is the normalized gravitational force and torque vector at the initial position (θ_0/f_n). Since it lies inside the limit surface, no sliding happens and the position and orientation of the object does not change.

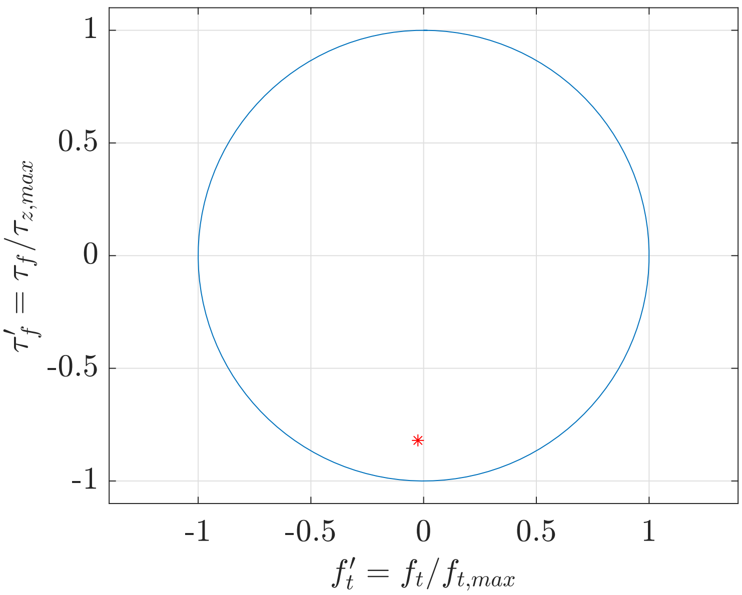

Figure 3.6: The normalized limit surface $(f_t',\ \tau_f') = (f_t/f_{t,max},\ \tau_f/\tau_{z,max})$. The red point is the normalized gravitational force and torque $(f_g',\ \tau_g') = (f_g/2f_{t,max},\ \tau_g/2\tau_{z,max})$ at the initial position with $f_n = 20\,\mathrm{N}$.

With a changed normal force $f_n = 15\,\mathrm{N}$, the normalized force and torque vector lies outside the limit surface (Figure 3.7). A rotating movement happens, which can be seen in Figure 3.8. The plot shows the angle θ and the translational motion of the grasped object. The blue curve is is the result of the combined model and the red curve the one of the rotational model. Both curves are nearly identical for the rotational motion. They start at the initial orientation of $\theta_0 = 27°$ and end at an angular position of $-84°$ after 0.7 seconds.

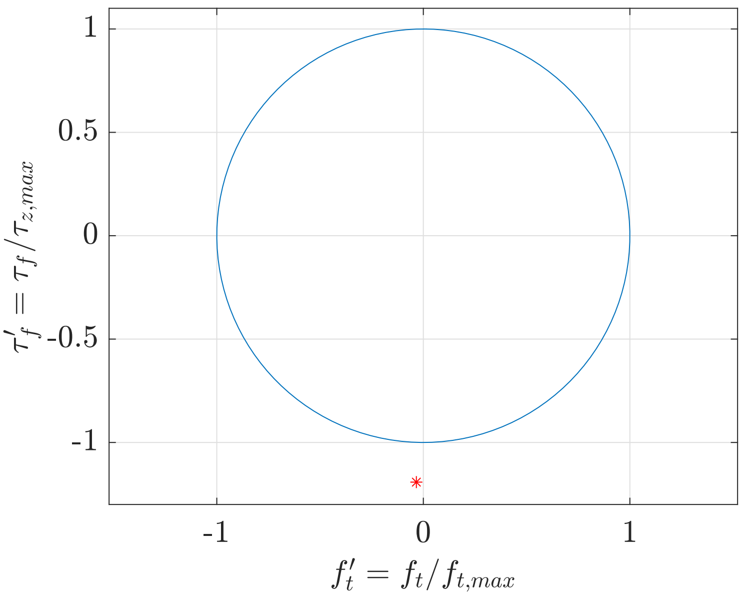

Figure 3.7: The normalized limit surface $(f_t',\ \tau_f') = (f_t/f_{t,max},\ \tau_f/\tau_{z,max})$. The red point is the normalized gravitational force and torque $(f_g',\ \tau_g') = (f_g/2f_{t,max},\ \tau_g/2\tau_{z,max})$ at the initial position with $f_n = 15\,\mathrm{N}$.

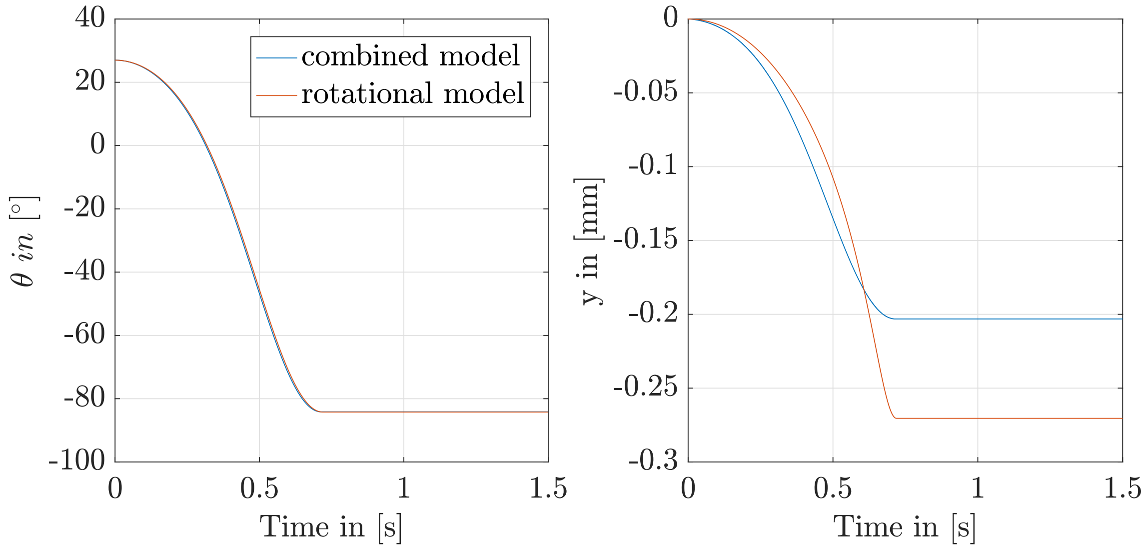

Figure 3.8: Angular orientation and displacement in y-direction of the grasped object with a constant grasping force $f_n = 15\,\mathrm{N}$ and an initial orientation of $\theta_0 = 27°$.

For the translational motion of the combined model the object is displaced by around $-0.2\,\mathrm{mm}$ and for the rotational model it is moved by $-0.27\,\mathrm{mm}$. Both motions happen in the first 0.7 seconds like the rotational motion.
The gravitational force is very small compared to the gravitational torque and therefore, the displacement of the object in y-direction is very small. The difference of both models can be explained because the rotational model calculates the translational motion depended on the rotational velocity (3.21), while the combined model uses translational dynamics for the translational motion (3.26).

3.2.2 Additional external force and torque

To force the system to do certain rotational or translational movements, an additional external torque τ_{ext} and force f_{ext} are applied to the contact point (Figure 3.9). We define the cumulative external force and torque as $f_{sum} = f_g + f_{ext}$ and $\tau_{sum} = \tau_g + \tau_{ext}$ respectively.

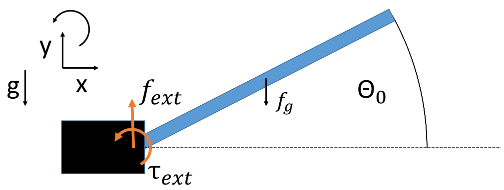

Figure 3.9: Modeling of the pivoting task with an additional external force f_{ext} and torque τ_{ext}.

Both the rotational and the combined model have to be modified. To calculate the frictional force and torque, Eq. (3.10) and (3.11) are rewritten as

$$f'_t = \begin{cases} \sin(\arctan(f'_{sum}/\tau'_{sum}) - \pi), & (v_t \neq 0 \lor |f_{sum}| \geq |2f_t|) \land (f'_{sum} < 0,\ \tau'_{sum} < 0) \\ \sin(\arctan(f'_{sum}/\tau'_{sum})), & (v_t \neq 0 \lor |f_{sum}| \geq |2f_t|) \land \neg(f'_{sum} < 0,\ \tau'_{sum} < 0) \\ -f'_{sum}, & (v_t = 0 \land |f_{sum}| < |2f_t|) \end{cases} \tag{3.27}$$

$$\tau'_f = \begin{cases} \cos(\arctan(f'_{sum}/\tau'_{sum}) - \pi), & (\dot{\theta} \neq 0 \lor |\tau_g| \geq 2|\tau_f|) \land (f'_{sum} < 0,\ \tau'_{sum} < 0) \\ \cos(\arctan(f'_{sum}/\tau'_{sum})), & (\dot{\theta} \neq 0 \lor |\tau_g| \geq 2|\tau_f|) \land \neg(f'_{sum} < 0,\ \tau'_{sum} < 0) \\ -\tau'_{sum}, & (\dot{\theta} = 0 \land |\tau_{sum}| < 2|\tau_f|) \end{cases} \tag{3.28}$$

where

$$f'_{sum} = (f_g + f_{ext})/2f_{t,max}$$
$$\tau'_{sum} = (\tau_g + \tau_{ext})/2\tau_{z,max}.$$

The rotational model is modified by rewriting the rotational and translational dynamics given by (3.18) and (3.21)

$$I\ddot{\theta} = \begin{cases} \tau_{sum} - sign(\tau_{sum})2|\tau_f|, & \dot{\theta} = 0 \\ \tau_{sum} - sign(\dot{\theta})2|\tau_f|, & \dot{\theta} \neq 0 \end{cases} \tag{3.29}$$

$$ma_y = \begin{cases} f_{sum} - sign(f_{sum})2|f_t|, & v_y = 0 \\ f_{sum} - sign(v_y)2|f_t|, & v_y \neq 0. \end{cases} \tag{3.30}$$

For the combined model the friction force vector becomes

$$f_c = \begin{cases} \frac{\boldsymbol{A}^{-1}\Delta \boldsymbol{v}}{\sqrt{\Delta \boldsymbol{v}^\top \boldsymbol{A}^{-1}\Delta \boldsymbol{v}}}, & \Delta \boldsymbol{v} \neq 0 \\ -\frac{1}{2}\boldsymbol{g}_{sum}, & \sqrt{{f'_{sum}}^2 + {\tau'_{sum}}^2} \leq 1 \wedge \Delta \boldsymbol{v} = 0 \\ \frac{\boldsymbol{A}^{-1}\boldsymbol{r}_{ft,ext}}{\sqrt{\boldsymbol{r}_{ft,ext}^\top \boldsymbol{A}^{-1}\boldsymbol{r}_{ft,ext}}}, & \sqrt{{f'_{sum}}^2 + {\tau'_{sum}}^2} > 1 \wedge \Delta \boldsymbol{v} = 0 \end{cases} \tag{3.31}$$

where $\boldsymbol{g}_{sum} = [0 \quad -mg + f_{ext} \quad -mgl_{Center}\cos\theta + \tau_{ext}]^\top$. The force and torque ratio (3.25) is adapted to

$$\boldsymbol{r}_{ft,ext} = [0 \quad |\lambda \frac{f'_{sum}}{\tau'_{sum}}| \quad -sign(\tau_{sum})]^\top. \tag{3.32}$$

The combined dynamics of Eq. (3.26) can be rewritten as

$$\ddot{\boldsymbol{q}} = \begin{cases} \boldsymbol{M}^{-1}(2\frac{\boldsymbol{A}^{-1}\Delta \boldsymbol{v}}{\sqrt{\Delta \boldsymbol{v}^\top \boldsymbol{A}^{-1}\Delta \boldsymbol{v}}} + \boldsymbol{g}_{sum}), & \Delta \boldsymbol{v} \neq 0 \\ 0, & \sqrt{{f'_{sum}}^2 + {\tau'_{sum}}^2} \leq 1 \wedge \Delta \boldsymbol{v} = 0. \\ \boldsymbol{M}^{-1}(2\frac{\boldsymbol{A}^{-1}\boldsymbol{r}_{ft,ext}}{\sqrt{\boldsymbol{r}_{ft,ext}^\top \boldsymbol{A}^{-1}\boldsymbol{r}_{ft,ext}}} + \boldsymbol{g}_{sum}), & \sqrt{{f'_{sum}}^2 + {\tau'_{sum}}^2} > 1 \wedge \Delta \boldsymbol{v} = 0 \end{cases} \tag{3.33}$$

In the first scenario the external force is set to zero and the external torque τ_{ext} is defined by the user and is shown in Figure 3.10. The other curves in this plot are the gravitational torque τ_g, the total external torque τ_{sum} and the corresponding minimal and maximal frictional torque while pivoting with a constant gripping force of 15 N, using the rotational model and the object parameters of Table 3.1.

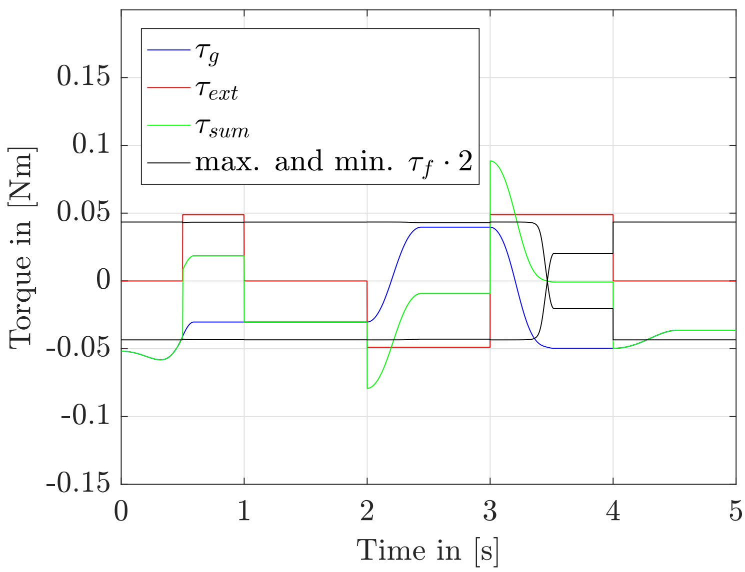

Figure 3.10: Occurring torques while pivoting with an external torque for the rotational model. The blue curve shows the gravitational torque, the red curve is the external torque. Adding the previous torques leads to the green curve. The black lines are the minimal and maximal frictional torques cause by an gripping force of 15 N.

The first 0.5 seconds the external torque is zero. The gravitational torque is smaller than the minimal frictional torque. Thus, the object accelerates in negative direction, which can be seen in Figure 3.12. After 0.5 seconds there is applied a positive external torque, which is added with the gravitational torque in between the minimal and maximal torque. Hence, there is a positive angular acceleration until the angular velocity is zero. τ_{sum} is inside of the minimal and maximal frictional torque. Therefore, θ is not changing until 2 seconds. At this point τ_{sum} is smaller than the minimal frictional torque and the object accelerates in negative direction. At around 2.2 seconds, τ_{sum} gets bigger than the minimal frictional torque. The object is accelerated until its velocity is zero. The same procedure happens at 3 and 4 seconds. The object gets accelerated first and than decelerated until it stops. The maximal and minimal frictional force changes because it depends on the limit surface. The closer the cumulative external torque τ_{sum} is to zero the smaller is the magnitude of the frictional torque.

Figure 3.11 shows the same as Figure 3.10 just for the combined model. All torques look similar the rotational model in Figure 3.10. However, there are some minor differences, which lead to a cumulative external torque τ_{sum} very close to zero for the rotational model from 3.2 seconds to 4 seconds (Figure 3.10) and a little bit bigger τ_{sum} for the combined model (Figure 3.11). Hence, the magnitude of the maximal and minimal frictional torque is bigger for the combined model than for the rotational model.

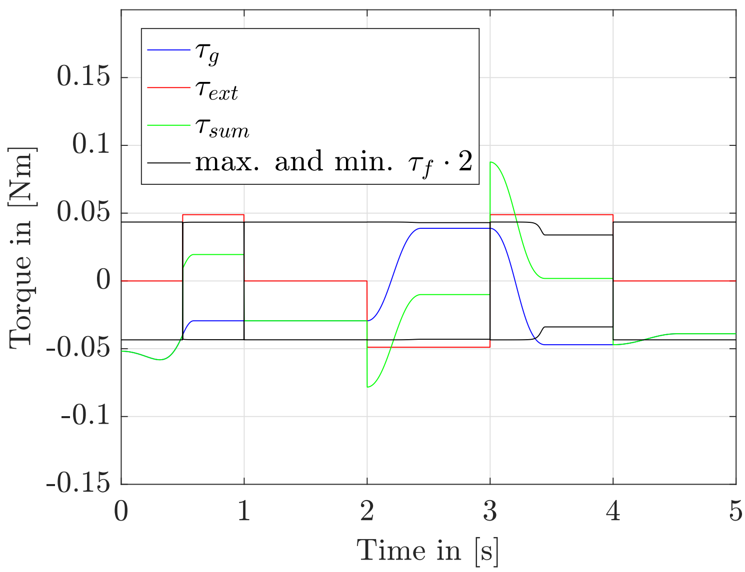

Figure 3.11: Occurring torques while pivoting with an external torque for the combined model. The blue curve shows the gravitational torque, the red curve is the external torque. Adding the previous torques leads to the green curve. The black lines are the minimal and maximal frictional torques caused by a gripping force of 15 N.

This affects the angular and translational position. From Figure 3.12 can be seen that for the first 3.2 seconds the angular position of the object for both models are very similar. After 3.2 seconds, the combined model is more damped than the rotational model. This can be attributed to the bigger magnitude of the maximal and minimal frictional torque.

The displacement of the object in y-direction can be seen in the right plot of Fig. 3.12. As in Figure 3.8 the motions of both models are different here as well. Both models have a translational motion always if the angular positing is changed. However, the amount differs.

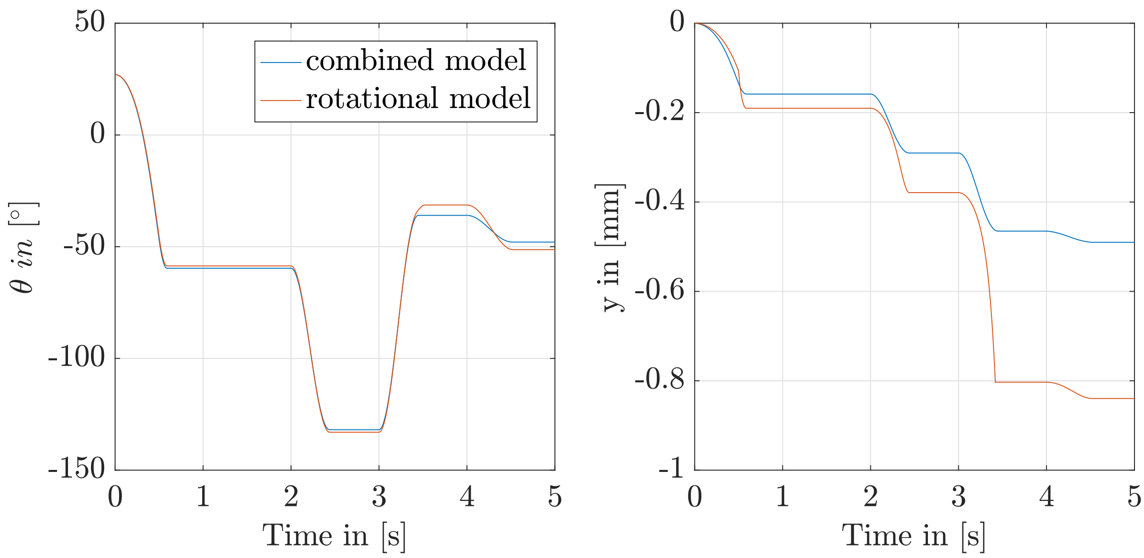

Figure 3.12: Angular orientation and translational motion of the grasped object with a constant grasping force $f_n = 15\,\mathrm{N}$, an initial orientation of $\theta_0 = 27°$ and a changing external torque, which can be seen in Figure 3.10.

The combined model has a smoother, more damped curve with a total displacement of $-0.5\,\mathrm{mm}$. The curve of the rotational model is less damped. Its total displacement in y-direction is around $-0.85\,\mathrm{mm}$. Since the gravitational force is always in negative y-direction, the displacement is also always in negative y-direction.

For the second scenario we apply an external force and an external torque, which are displayed in Figure 3.13 and Figure 3.14 respectively. The pivoting is performed with the object parameters of Table 3.1, a constant gripping force of $5\,\mathrm{N}$ and an initial angular position of $\theta_0 = 90°$.

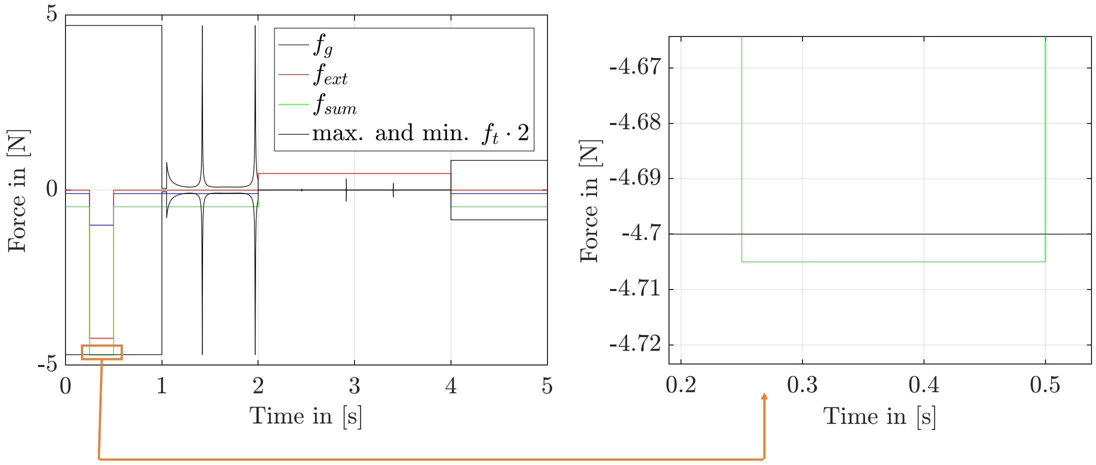

Figure 3.13: Occurring forces while pivoting with an external force and torque for the combined model. The right plot shows the orange sector of the left plot zoomed in. The black lines are the minimal and maximal frictional forces caused by a gripping force of 5 N.

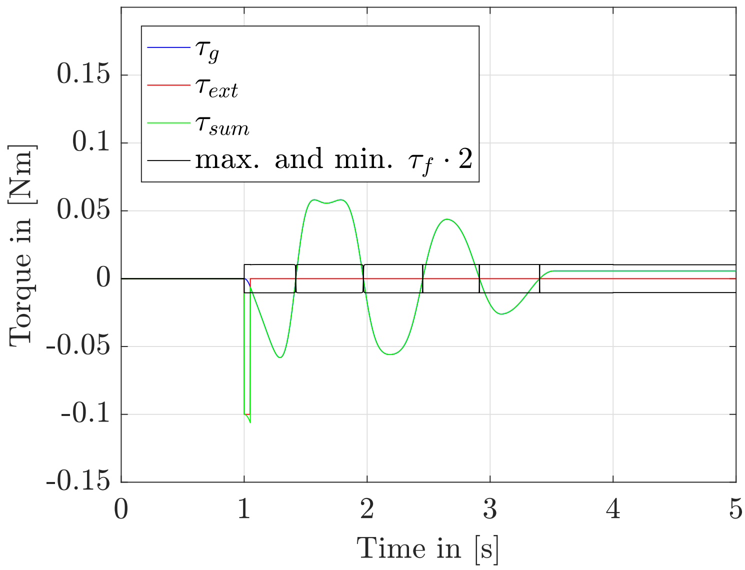

Figure 3.14: Occurring torques while pivoting with an external force and torque for the combined model. At 1 second a negative external pulse is given. After that, $\tau_{sum} = \tau_g$. The black lines are the minimal and maximal frictional torques caused by a gripping force of 5 N.

In the first 0.25 seconds $\tau_{sum} = 0$ and $f_{sum} = 0$ lies inside of the maximal and minimal frictional force from both fingertips. Thus, no movement happens. Between 0.25 and 0.5 seconds an external force is applied such that f_{sum} is smaller than the minimal frictional force. The object starts moving in negative y-direction (Figure 3.15). After that the object is decelerated until its velocity is zero. At 2 seconds, an external torque pulse is applied to the object. The object starts rotating and swings around $\theta = -90°$ until its energy is totally dissipated and it stops at 3.5 seconds. Additionally, the object moves in negative y-direction due to the gravitational force. At 2 seconds an external force is applied, which compensates the gravitational force. Hence, the object stops its translational motion. The occurring torques and forces for the rotational model are very similar to the ones of the combined model. The corresponding plots can be seen in Figures A.1 and A.2.

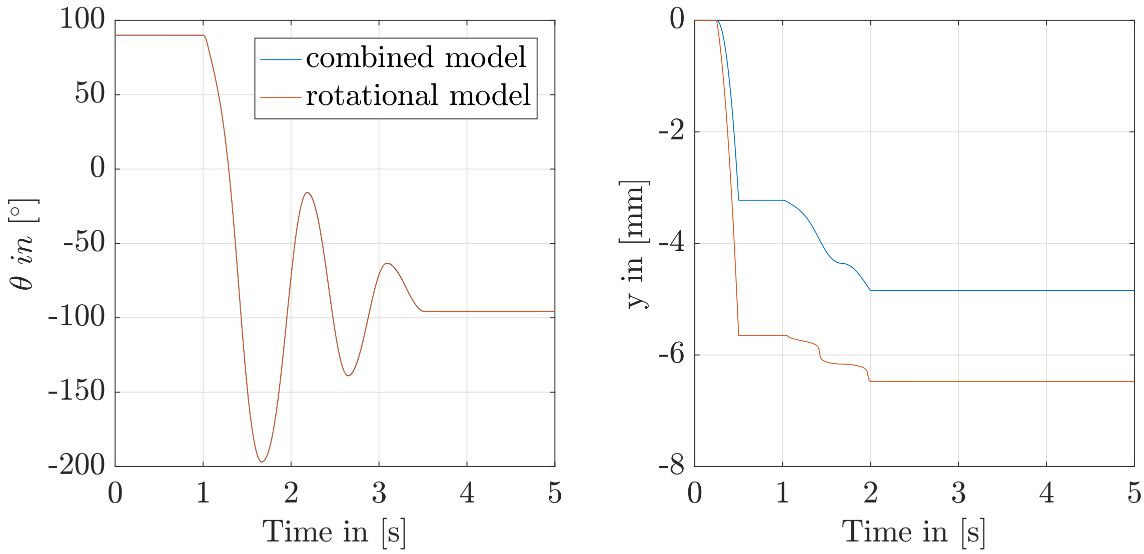

Figure 3.15: Angular orientation and displacment in y-direction of the grasped object with a constant grasping force $f_n = 5\,\mathrm{N}$, an initial orientation of $\theta_0 = 90°$ and a changing external force and torque, which can be seen in Fig. 3.13 and 3.14.

Figures 3.15 shows the angular and y-position of the object while pivoting with this scenario. For the rotational movement both models are identical. However, the displacement in y-direction has differences, which are very similar to the discussed differences of Figure 3.12. The motions happen at the same time for both models, but the the rotational model has a bigger displacement.

To conclude this section, we have derived two different contact models, which are both based on the concept of the limit surface. The first model, the rotational model, uses the frictional torque calculated directly from the limit surface for the rotational dynamics. The translational velocity is calculated by a ratio between the rotational and the translational velocity. Only if the cumulative external torque is smaller than the cumulative external force, the translational dynamics are calculated with the frictional force from the limit surface. The second model, the combined model, using a velocity depended frictional force and torque for the rotational and translational dynamics.
The simulation results show that both models have a very similar behavior for the angular position of the object while pivoting. However, the displacements' response in y-direction have some differences. In the shown scenarios the displacements of

the rotational model are bigger than the displacements of the combined model. The difference between the models can be attributed to the way that the translational velocity is calculated. The results of the combined model can be seen as more accurate, because this model uses real dynamics while the rotational model just calculates the translational velocity as a function of the rotational velocity.

3.3 Control Problem

The aim of this thesis is to control the normal force, which is applied from the fingertips to the object, in an appropriate way such that the orientation of the object is changed in a desired way. Since it is only performed passive pivoting with the help of gravity, the object will always rotate in only one direction. Hence, no overshooting is tolerable. To achieve this, the trajectory of the object should follow a reference trajectory, which is generated with a critical damped second order system. The overall system with its subsystems is graphically illustrated in Fig. 3.16.

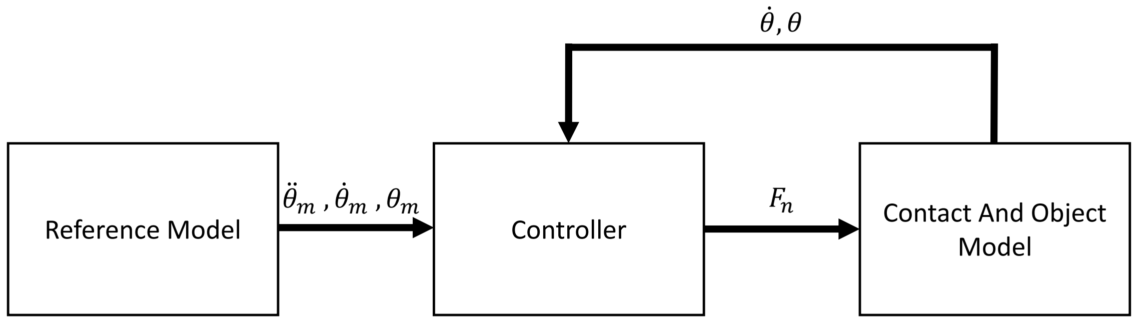

Figure 3.16: The simulation model contains three subsystems: The reference model provides the desired trajectory of the object, the controller calculates the normal force to follow this trajectory and the contact and object model is the plant, which contains the object dynamics and the contact between the gripper and the object.

Since the torsional friction coefficient is difficult to measure, it is seen as a uncertain parameter. To get good results without knowing the exact value of the friction coefficient, an adaptive control design introduced in Section 2.3 can be contrived. Another possible solution to deal with the uncertainty of the torsional friction coefficient is to derive a model free controller proposed in Section 2.4. This control approach is independent of the model dynamics, instead it only depends on prescribed performance bounds concerning the tracking error. The translational motion is not considered for the control approach, however, it is desirable to find the smallest possible translational displacement.

3.3.1 Delimitation

For simplicity, we consider the in-hand manipulation task as planar problem. Moreover, centrifugal forces generated through the motion of the object are seen as negligible because they are very small compared to the gravitational force applied through the mass of the object. It is assumed that we can control the normal force of the fingertips directly and that we can measure the position and velocity of the object without any sensor noise. The object is assumed as rigid without any deformations.

4
Control Design

In this chapter, two different control approaches are applied to design controllers for regulating the actual orientation of the object to a desired orientation.
For the control design several assumptions are made:

1. The inertial parameters (I, m, l_{center}) of the object are known but for the torsional friction coefficient μ_{tors} small uncertainties are allowed. The initial parameters can be gathered from experiments using e.g. wrist-mounted force-torque sensor before the pivoting task is performed [23]. In practice it is difficult to measure the torsional friction coefficient μ_{tors}. Therefore, the use of an adaptive controller with adaption on μ_{tors} is justified.
2. The angular position and the angular velocity can be gathered from the contact model.
3. The robot's gripper is force controlled and is modelled without errors. That means the desired normal force f_n is directly applied to the grasped object.
4. The gripper is oriented such that the gravitational torque can rotate the object to the desired end position, i.e. $sgn(\tau_g) = sgn(\theta_d - \theta_0)$.
5. the parameter γ from the soft finger model depends on the material of the fingertips and can be estimated offline. Therefore, this parameter is assumed as known.
6. Since we perform passive pivoting, the angular position θ must not overshoot.

The control structure can be seen in Fig. 3.16. The reference model has the desired angular position, velocity and acceleration as output and the controller controls the normal force of the gripper.
We define the system's state $x(t) = [\theta(t),\ \dot{\theta}(t)]$, which is driven along a state trajectory $x_m(t) = [\theta_m(t),\ \dot{\theta}_m(t)]$ by the controller. The state trajectory is characterized by a reference model, which is defined by the user and describes the optimal response that the system should follow. Since we want to avoid an overshoot in the angular position response, we design the reference model as a critically damped second order system [24] with the following transfer function

$$H_m(p) = \frac{\theta_m}{\theta_{in}} = \frac{\lambda_0^2}{(p + \lambda_0)^2} \tag{4.1}$$

where the reference input θ_{in} has a trapezoidal velocity profile.

First, we introduce a simplified rotational object dynamic model where the theory of Section 2.3 can be applied. The rotational dynamics are given by the following equation:

$$I\ddot{\theta} = \tau_g + 2\mu_{tors} f_n^{1+\gamma}. \tag{4.2}$$

For the rotational model the rotational dynamics are given by Eq. (3.19). By substituting Eq. (3.9) we get

$$I\ddot{\theta} = \tau_g + 2\mu_{tors} \left| \cos\left(\arctan\left(\frac{f'_g}{\tau'_g} \right) \right) \right| f_n^{1+\gamma} \tag{4.3}$$

where f'_g and τ'_g are the normalized gravitational force and torque given by Eq. (3.12) and Eq. (3.13).
The rotational dynamics of the combined model are given by the third component of the combined dynamics of Eq. (3.26) and can be written as

$$I\ddot{\theta} = \tau_g - 2 \frac{\dot{\theta}\mu_{tors}^2 f_n^{\gamma}}{\sqrt{v_y^2 \mu^2 + \dot{\theta}^2 \mu_{tors}^2 f_n^{2\gamma}}} f_n^{1+\gamma}. \tag{4.4}$$

Equations (4.2) - (4.4) can be rewritten as follows:

$$f_n^{1+\gamma} = h_* \ddot{\theta} + b_* \tau_g \tag{4.5}$$

where $h_* \in \{h_{simpl}, h_{rot}, h_{comb}\}$ and $b_* \in \{b_{simpl}, b_{rot}, b_{comb}\}$ are parameters of the simplified dynamics, the rotational model and the combined model, which are defined as:

$$h_* = \begin{cases} 0.5 I \mu_{tors}^{-1}, & h_* = h_{simpl} \\ \frac{I}{2\mu_{tors} \left| \cos\left(\arctan\left(\frac{f'_g}{\tau'_g} \right) \right) \right|}, & h_* = h_{rot} \\ -\frac{I\sqrt{v_y^2 \mu^2 + \dot{\theta}^2 \mu_{tors}^2 f_n^{2\gamma}}}{2\dot{\theta}\mu_{tors}^2 f_n^{\gamma}}, & h_* = h_{comb} \end{cases} \tag{4.6}$$

$$b_* = \begin{cases} -0.5 \mu_{tors}^{-1}, & b_* = b_{simpl} \\ -\frac{1}{2\mu_{tors} \left| \cos\left(\arctan\left(\frac{f'_g}{\tau'_g} \right) \right) \right|}, & b_* = b_{rot} \\ \frac{\sqrt{v_y^2 \mu^2 + \dot{\theta}^2 \mu_{tors}^2 f_n^{2\gamma}}}{2\dot{\theta}\mu_{tors}^2 f_n^{\gamma}}, & b_* = b_{comb} \end{cases} \tag{4.7}$$

It is notable that Eq. (4.5) is not a explicit notation of the normal force for the rotational and the combined model since the normalized force and torque f'_g and τ'_g depend on the normal force. Also, the control theory of Section 2.3 can only be applied directly to the simplified object dynamics. For the rotational and the combined model some assumptions have to be made. The parameters h_{rot}, h_{comb}, b_{rot} and b_{comb} are not constant during pivoting. They depend on the normal force and the object orientation.
If v_y converges to zero, $h_{comb} = h_{simpl} = 0.5 I \mu_{tors}^{-1}$ and $b_{comb} = b_{simpl} = -0.5\mu_{tors}^{-1}$. If v_y converges to infinity, h_{comb} and b_{comb} converge to plus or minus infinity as well. Hence, the parameters are bounded at one side with the minimal absolute value for $v_y = 0$. The bounds of the parameters h_{rot} and b_{rot} are similar since $\left| \cos\left(\arctan\left(\frac{f'_g}{\tau'_g} \right) \right) \right| \in [0 \quad 1]$.

Since the parameters of the rotational model h_{rot} and b_{rot} are slow changing if the gravitational torque is much bigger than the gravitational force and parameters h_{comb} and b_{comb} of the combined model are nearly constant if v_y is very small, we assume that the control approach of Section 2.3 is still valid for most of the pivoting tasks. The validity and limits of this assumptions is shown by simulation in Chapter 5.
The tracking control error s is defined as

$$s = \dot{\tilde{\theta}} + \lambda\tilde{\theta} \tag{4.8}$$

where $\tilde{\theta} = \theta - \theta_m$ is the the angular position error, $\dot{\tilde{\theta}} = \dot{\theta} - \dot{\theta}_m$ is the angular velocity error and λ is a constant.

4.1 Adaptive controller

The adaptive control design follows the strategy of [6]. A model reference adaptive control is considered to perform the pivoting task with errors in the torsional friction coefficient μ_{tors}, which represents parametric uncertainties in the nonlinear models (4.2) - (4.4).

We formulate the standard adaptive control law [9]

$$f_n^{1+\gamma} = \hat{h}_*\ddot{\theta}_r - k_s s + \hat{b}_*\tau_g \tag{4.9}$$

where the reference angular acceleration $\ddot{\theta}_r = \ddot{\theta}_m - \lambda\dot{\tilde{\theta}}$ multiplied with $\hat{h}_*$ is a velocity error and feed-forward acceleration term, $k_s s$ is a tracking error term and $\hat{b}\tau_g$ is a nonlinear gravity compensation term. k_s is a positive control gain and $\hat{h}_*, \hat{b}_*$ are adaptive estimates of h_* and b_* given by

$$\dot{\hat{h}}_* = -\alpha_h s\ddot{\theta}_r \tag{4.10}$$

$$\dot{\hat{b}}_* = -\alpha_b s\tau_g \tag{4.11}$$

where α_h and α_b are positive adaption gains. The initialization of h_* and b_* is done with an estimated torsional friction coefficient and Eq. (4.6) and (4.7). It is notable that for the initialization of $\hat{h}_{comb}$ and $\hat{b}_{comb}$, v_y is substituted with $-\left|\lambda\frac{f_y'(0)}{\tau_g'(0)}\right|$ and $\dot{\theta}$ is substituted with $sign(\cos\tau_g)$ in Eq. (4.6) and (4.7). This is done the same as in Section 3.1.3 since h_{comb} and b_{comb} are not defined for velocities equals to zero.
It is important to mention that the adaptation estimates calculated online with (4.10) and (4.11) are not guaranteed to converge to the correct values unless continuous excitation. However, the control design does guarantee convergence of the tracking error s. This implies that the orientation of the object converges to the desired orientation.

4.2 Model free controller

The torsional friction coefficient is seen as uncertain and therefore, it is difficult to apply a controller which depends on the model dynamics. The adaptive controller of the previous chapter can adapt the torsional friction coefficient, however, we had to make some assumptions, which limit the working range of the controller. In this section, a model free controller is derived, which is based on the idea of Section 2.4 and guarantees prescribed performance.

We want to follow the reference trajectory defined in (4.1), which leads to the combined tracking error s defined in (4.8). To achieve prescribed performance, following equation has to be satisfied $\forall t \geq 0$:

$$\underline{b}(t) < s < \overline{b}(t) \tag{4.12}$$

where the performance bounds $\underline{b}(t)$, $\overline{b}(t)$ are defined in Section 2.4 and illustrated in Fig. (2.6).

The theory of Section 2.4 cannot be applied to our control problem directly, since it is only valid for a class of models which have an input range of $u \in (-\infty, \infty)$. The contact model between the robot hand and the object with the normal force as input is limited to $f_n \in [0, \infty)$. Therefore, we have to employ a different error transformation function $T(\cdot)$, which is smooth and strictly increasing.

$$\xi = T(\hat{s}) \tag{4.13}$$

$$T : \Omega \to (-\infty, 0) \tag{4.14}$$

where ξ is the transformed error and $\hat{s} = \frac{s}{\rho}$ is the normalized tracking error. The open set Ω is defined in Section 2.4.

A candidate error transformation function which satisfies (4.14) is given by:

$$T(\hat{s}) = \frac{\hat{s} - 1}{M + \hat{s}} \text{ for } -M < \hat{s} \leq 1 \tag{4.15}$$

where the constant $M \in [0,\ 1]$. An illustration of (4.15) is shown in Fig. 4.1.

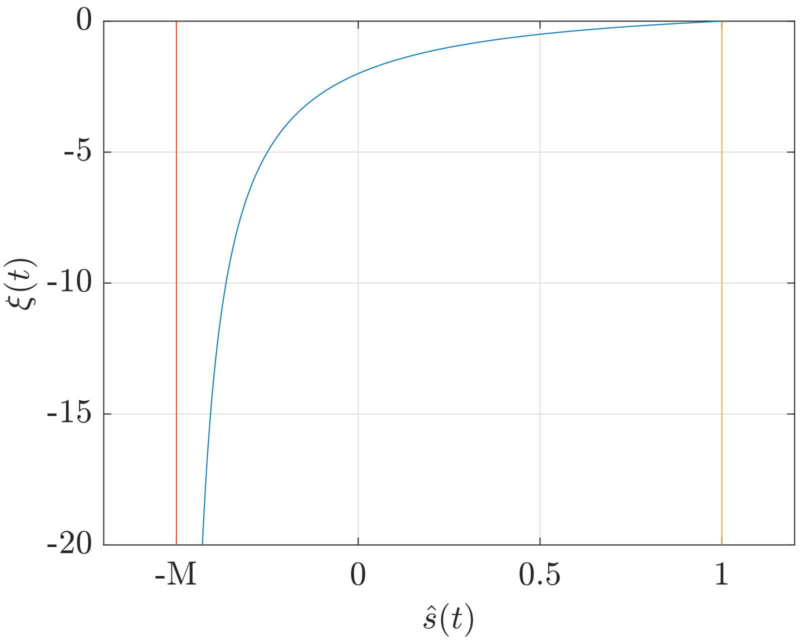

Figure 4.1: Illustration of the error transformation of Eq. (4.15).

The control input is then given by:

$$f_n = -K_{mf} J_{mf} \xi \tag{4.16}$$

where K_{mf} is a positive control gain and J_{mf} denotes the normalized slope of $T(\hat{s})$, which is given by:

$$J_{mf} = \frac{\partial T}{\partial \hat{s}} \frac{1}{\rho(t)} \tag{4.17}$$

It has to be noted that the initial error is limited by $-M < \hat{s}(0) \leq 1$. In Section 2.4 we have different error transformations for a normalized error bigger or smaller zero. In our case we have only one error transformation. Since we perform passive pivoting and we want to avoid an overshooting in negative direction, a small M is desirable. The here proposed control law is not proven mathematically, however, it is easy to see that the combined error always stays inside the bounds since the normal force increases to infinity if we reach the lower bound and converges to 0 if we reach the upper bound. Hence, the object cannot move further if the combined tracking error is close to the lower bound and the combined error remains constant or increases.

It is also possible to change the tracking error for the prescribed dynamics. By defining

$$e = \lambda(\theta - \theta_d) + \dot{\theta} \tag{4.18}$$

and replacing the combined tracking error s with e and $\hat{s}$ with $\hat{e} = \frac{e}{\rho}$ in all equations of Section 4.2, we relax the control constraints. The object does not follow any reference trajectory, instead only the position error to the desired end position and a penalization of the angular velocity is considered. Since we perform passive pivoting and every negative position error e means an irreversible overshoot of the desired position, the constant M is chosen close or equal to zero.

5
Results

This chapter shows the results of this thesis. The performance of the contact models derived in Section 3.1 in combination with the controllers of Section 4 is investigated and compared to each other. First, the adaptive control approach is considered. The adaptation gains α_h and α_b are set to zero to prevent an adaptation of the torsional friction coefficient. The torsional friction coefficient is assumed as know and therefore, the torsional friction coefficient of the controller is the same as for the contact model. After that the torsional friction coefficient is assumed as unknown. Hence, the controller and contact model use different torsional friction coefficients μ_{tors} and $\mu_{tors,m}$ respectively. The performance is investigated for both cases were the adaptation gains are set to zero and set bigger than zero for different desired trajectories and object parameters. Then the model free controller is considered and compared to the adaptive control approach for some in-hand manipulation tasks.

Table 5.1: Parameters of the object and contact model.

g [m/s^2]	9.81
m [g]	48.5
l_{center} [cm]	12.22
I [Kg $\cdot$ cm^2]	10.64
γ	0.3
μ	0.47
$\mu_{tors,m}$	$0.643 \cdot 10^{-3}$ or $0.85 \cdot 10^{-3}$
θ_0 [°]	27

Table 5.2: Parameters of the adaptive controller and for the reference model.

α_h	0 or 1.5
α_b	0 or $7.5 \cdot 10^{-3}$
k_s	23
λ	10
μ_{tors}	$0.643 \cdot 10^{-3}$
θ_d [°]	0
λ_0	2.5

Table 5.1 and 5.2 show the parameters used for the contact and object model and the adaptive controller. Each parameter, which has two different values, is changed

for the different scenarios.

5.1 Reference Trajectory

The reference angular position for the object is given by Eq. (4.1). For the parameters of Table 5.1 and 5.2 the trapezoidal input velocity of the reference model can be seen in Figure 5.1. Through integration the dotted blue line results, which is the input of the reference model. The blue line is the output of the reference model, which is the desired angular position of the object.

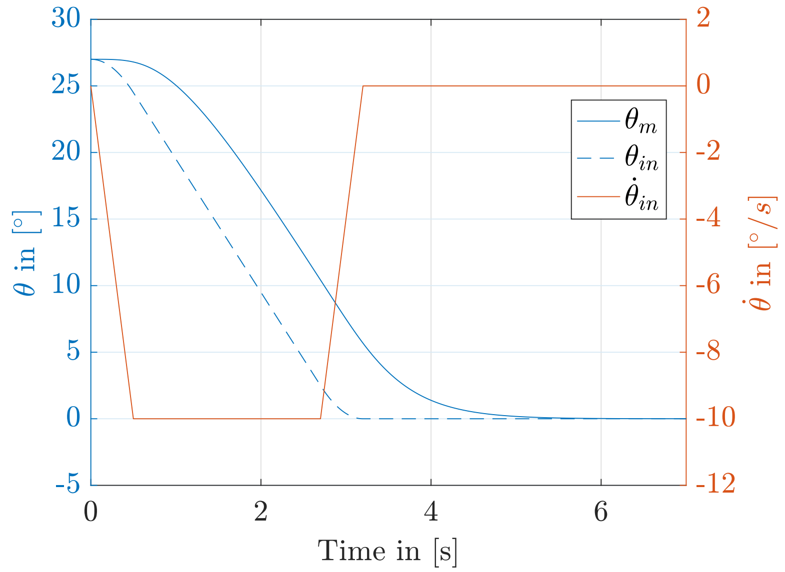

Figure 5.1: Reference signal: The blue line is the reference angular position θ_m which the object should follow. The dotted blue line is the input θ_{in} of the reference model given with Eq. (4.1). The red line is the trapezoidal input velocity $\dot{\theta}_{in}$ of the reference model.

5.2 Non-adaptive control

The controllers of Section 4.1 are first investigated without any adaptation of the torsional friction coefficient. The adaptation gains α_h and α_b are set to zero.

5.2.1 Equal friction coefficient

The torsional friction coefficient of the contact model and of the controller $\mu_{tors,m}$ and μ_{tors} respectively are both set to $0.643 \cdot 10^{-3}$. The behavior of the object for the rotational and the combined model can be seen in Figure 5.2 and Figure 5.3. Figure 5.2 shows the angular position of the object for both models and the desired trajectory as well as the normal force which is applied to the object.

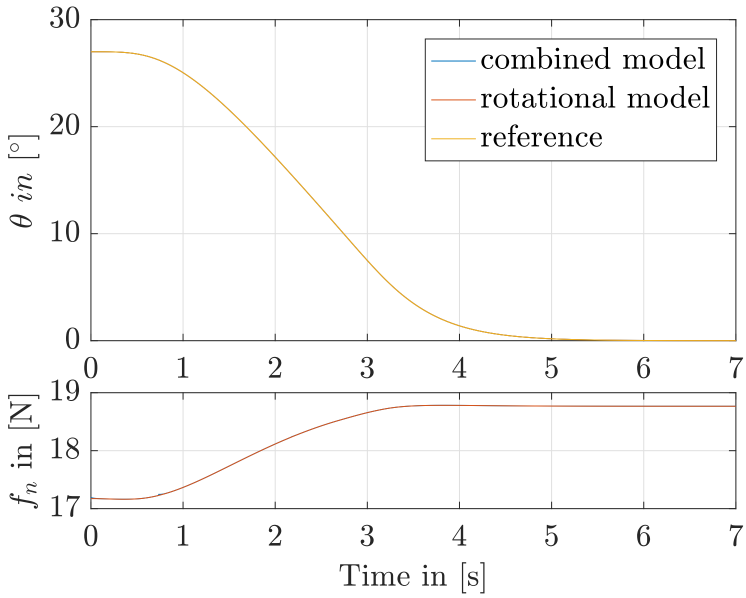

Figure 5.2: Angle of the object for the combined and the rotational model and desired reference angle for a known torsional friction coefficient and estimation gains α_h and α_b equal to zero (top). Normal force applied from the fingertips to the object (bottom).

Both models can follow the reference trajectory very well without overshooting the desired angular orientation. The applied normal force is very similar for both models. The displacement in y-direction while pivoting can be seen in Figure 5.3. Both models point out a very similar result. The displacement is with around -0.043 mm very small, which is good since we want to avoid translational sliding while pivoting.

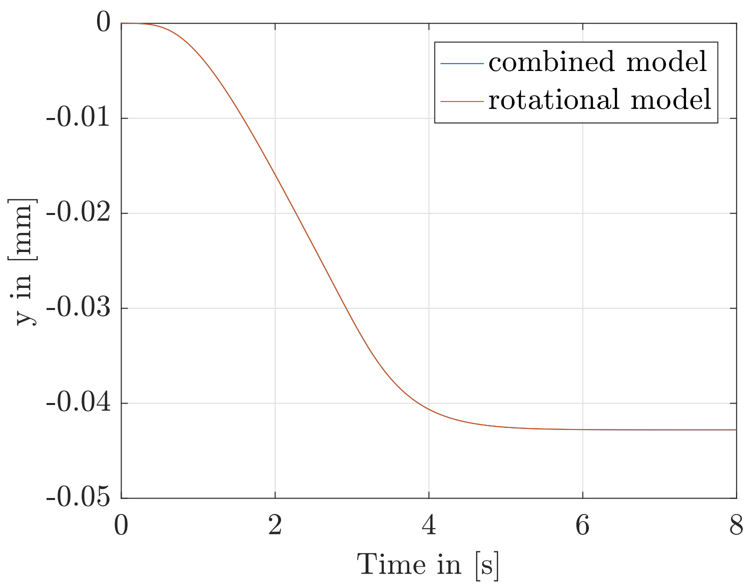

Figure 5.3: Sliding of the object in y-direction for the combined and the rotational model, while the object is manipulated from the initial to the desired angular orientation.

The translational motion is similar for both models although Section 3.2 pointed out a different behaviour of both models. Since the velocities while pivoting are much slower than the velocities in the uncontrolled cases of Section 3.2, we assume that there is only a different behaviour for the translational motion of both models for high velocities.

5.2.2 Uncertainty in the friction coefficient

Since the torsional friction coefficient is seen as uncertain, the torsional friction coefficient of the controller μ_{tors} is set different from the torsional friction coefficient of the contact model $\mu_{tors,m}$. The parameter μ_{tors} is set to $0.85 \cdot 10^{-3}$ while $\mu_{tors,m}$ remains at $0.643 \cdot 10^{-3}$. Figure 5.4 shows the angular position of the object while pivoting for both models, as well as the model reference and the normal forces. Since we cannot adapt the torsional friction coefficient, the object cannot follow the model trajectory and the angular position of the object ends at around 3° under the desired orientation.
The second plot shows the normal force which is applied to the object. The normal force is very similar for both models.

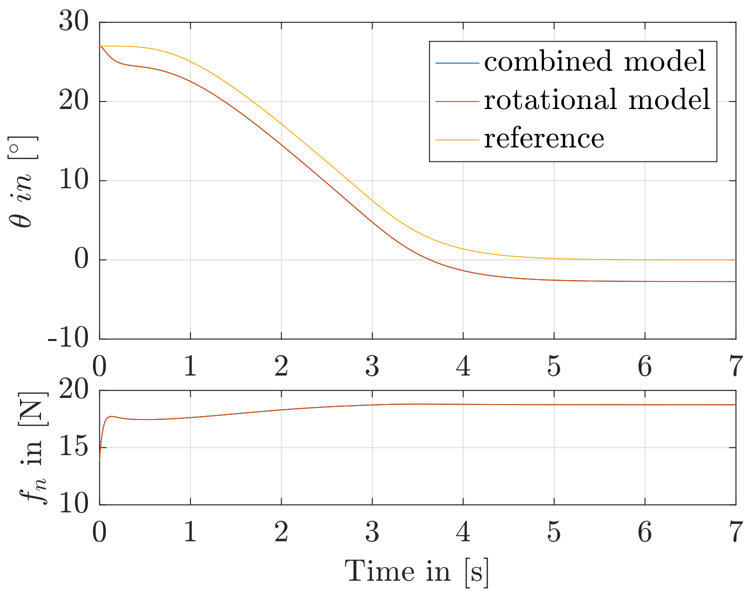

Figure 5.4: Angular position of the object for the combined and the rotational model and desired reference angle for an unknown torsional friction coefficient and estimation gains α_h and α_b equal to zero (top). The chosen torsional friction coefficients can be seen in Table 5.1 (second value) and Table 5.2. Normal force applied from the fingertips to the object (bottom).

The translational movements of the object for both models can be seen in Fig. 5.5. As the angular position, the displacement of the object is similar for both models. The total displacement is with around -0.047 mm bigger than in section 5.2. This can be attributed to the overshooting angular position and therefore, a bigger change for the orientation.

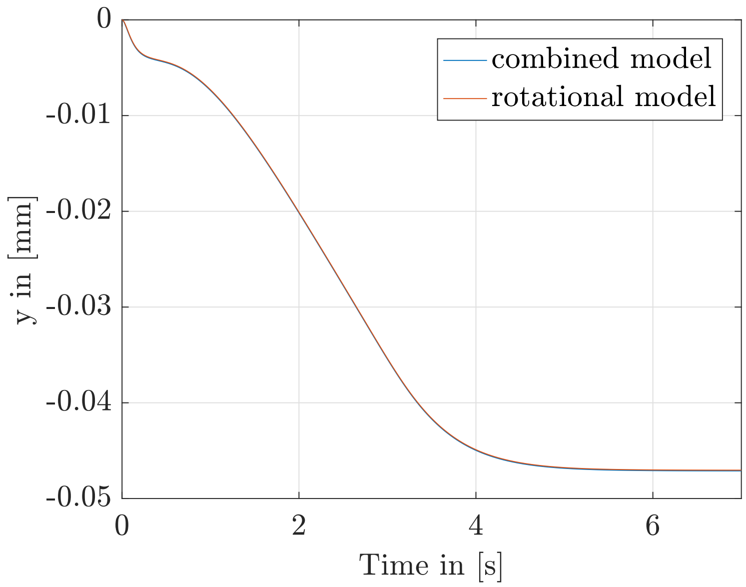

Figure 5.5: Sliding of the object in y-direction while the object is manipulated from the initial to the desired angular orientation for the combined and the rotational model.

5.3 Adaptive control

For the adaptive control the adaptive estimates $\hat{h}_{rot}$ and $\hat{b}_{rot}$ for the rotational model and $\hat{h}_{comb}$ and $\hat{b}_{comb}$ for the combined model have to be calculated with (4.6) and (4.7) by setting the adaptation gains bigger than zero. The adaptation gains are set to $\alpha_h = 1.5$ and $\alpha_b = 7.5 \cdot 10^{-3}$, which correspond to the second value of both parameters seen in Table 5.2.

5.3.1 Uncertainty in the friction coefficient

The torsional friction coefficient $\mu_{tors} = 0.85 \cdot 10^{-3}$ for the controller of both models is set the same as in Section 5.2.2 while using $\mu_{tors,m} = 0.643 \cdot 10^{-3}$ as parameter of the contact models (Table 5.1). Figure 5.6 shows the simulated trajectory of the angular position of the object for the rotational and the combined model and the desired trajectory. The trajectory of both models can reach the desired end orientation. Because of the erroneous initial torsional friction coefficient we get an error of the angular position in both models in the first 1.5 seconds.

The seconds plot shows the normal force which is applied to the object for both models. The normal force of both models are the same.

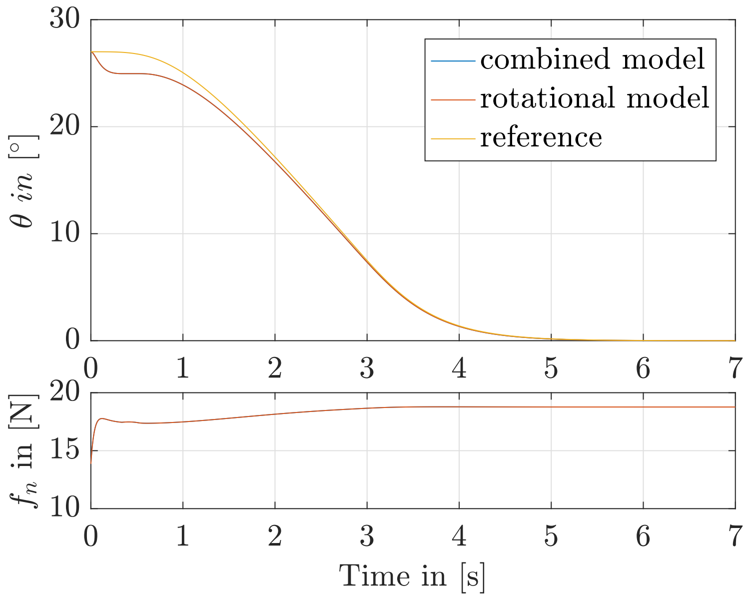

Figure 5.6: Angle of the object for the rotational and the combined model and desired reference angle for a different torsional friction coefficient for the model and the controller. The chosen torsional friction coefficients and the estimation gains α_h and α_b can be seen in Table 5.1 and Table 5.2 (second value). The second plot shows the applied normal force during the pivoting process for both models.

The parameters h_{comb}, h_{rot}, b_{comb} and b_{rot}, which are assumed as nearly constant and slow changing during pivoting, can be seen in Fig. 5.7.

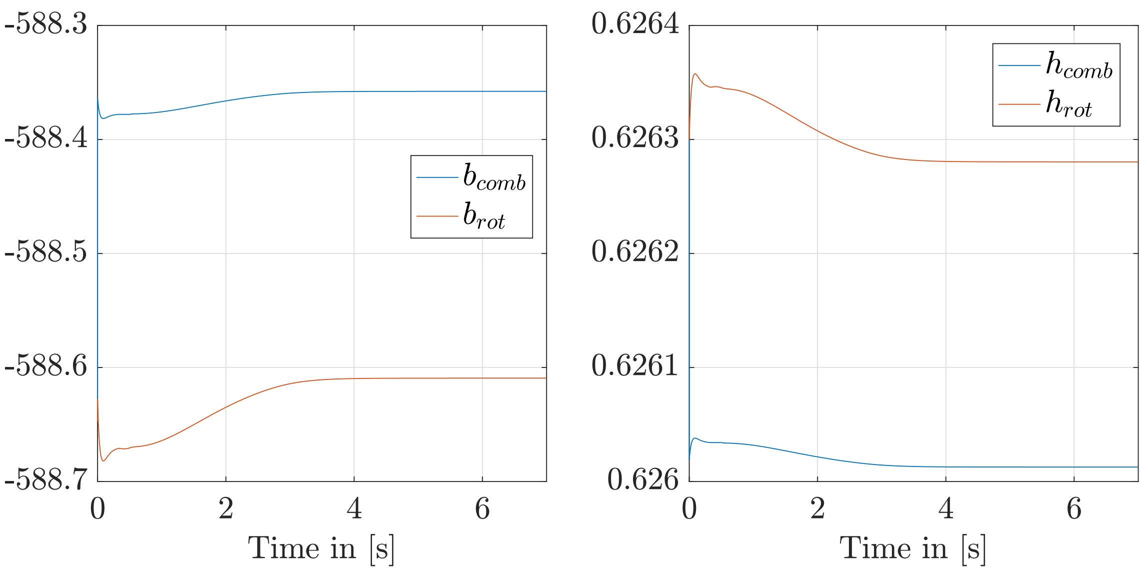

Figure 5.7: Parameters b_{comb} and h_{comb} of the combined model and b_{rot} and h_{rot} of the rotational model during pivoting.

All parameters vary only very slightly. For the combined model, h_{comb} and b_{comb} change in the beginning from the same values as h_{rot} and b_{rot}. This can be attributed to the fact that the combined model gets initialized with the same velocity ratio between the translational and the rotational velocity than the rotational model uses to calculate the translational motion during the whole process. After this jump in the beginning, the shape of the parameter evolution of both models look very similar. However, the parameters of the combined model change less. The assumption of slow changing parameters is therefore valid for this scenario. The values of the parameters of Fig. 5.7 at the time $t = 0$ initialize the estimated parameters $\hat{h}_{comb}$, $\hat{h}_{rot}$, $\hat{b}_{comb}$ and $\hat{b}_{rot}$.

Figure 5.8 shows the estimated parameters $\hat{b}_{comb}$ and $\hat{h}_{comb}$ of the combined model and $\hat{b}_{rot}$ and $\hat{h}_{rot}$ of the rotational model. As the angular position and the applied normal force, both models behave the same and the controller of each model estimate the parameters similar.

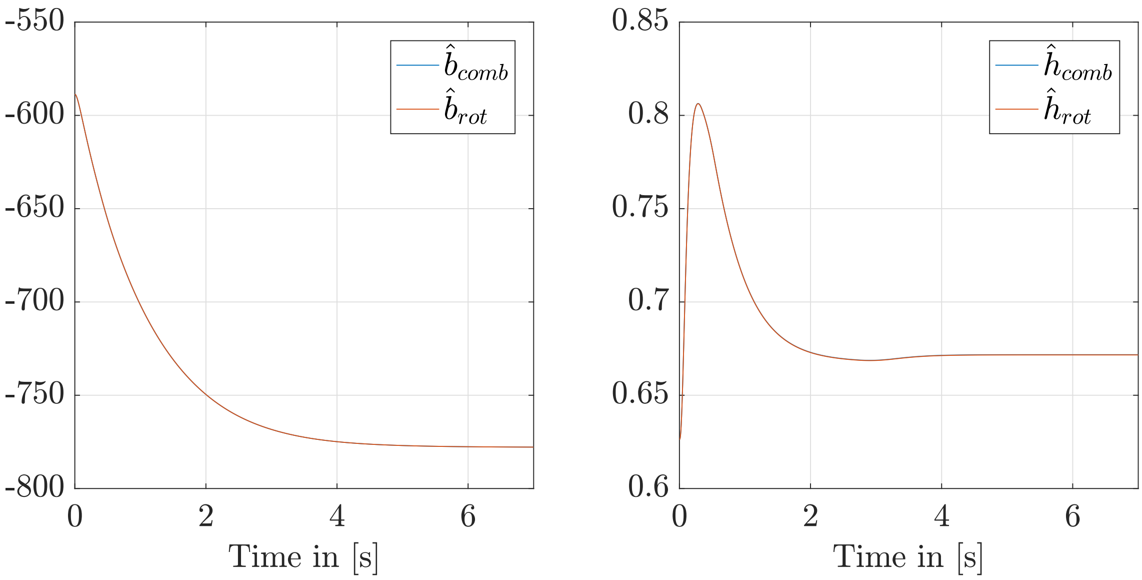

Figure 5.8: Estimation of $\hat{b}_{comb}$ and $\hat{h}_{comb}$ of the combined model and $\hat{b}_{rot}$ and $\hat{h}_{rot}$ of the rotational model during pivoting.

The displacement in y-direction and the adaption of the torsional friction coefficient for both models can be seen in Figure 5.9. The adaption of the torsional friction coefficient is calculated according to Eq. (4.7). Therefore, it depends directly on $\hat{b}_{comb}$ and $\hat{b}_{rot}$ of Fig. 5.8. Both models show the same behavior for the translational dynamics. The adaptation of the friction coefficient takes around 5 seconds to reach the value of the contact model. After that the torsional friction coefficient remains at this value.

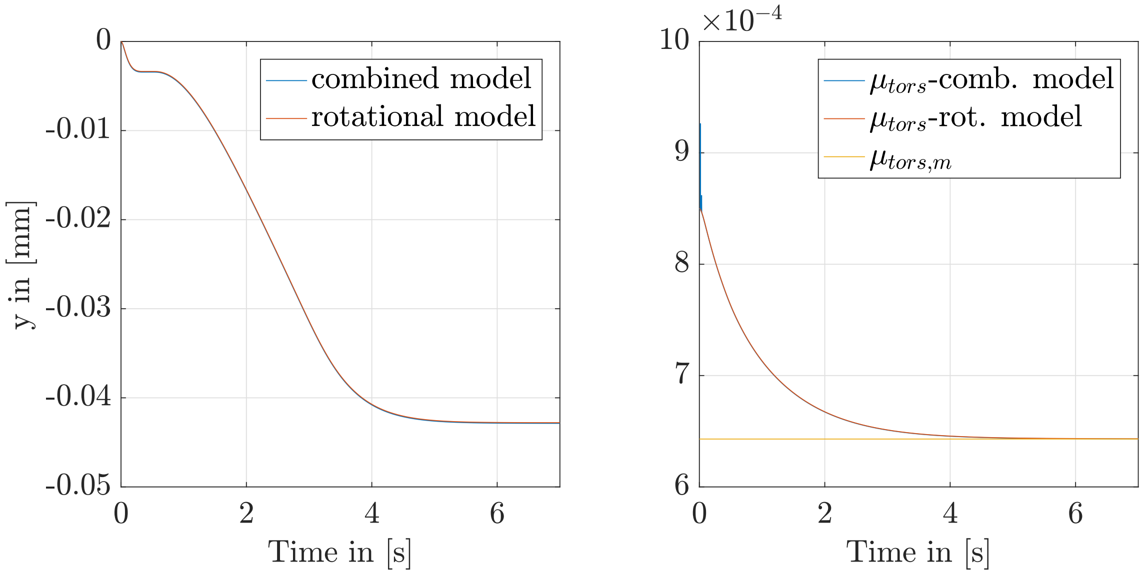

Figure 5.9: Adaptation of the torsional friction coefficient for the controller of the rotational and the combined model during pivoting. The yellow line is the coefficient which is used by the contact models, while the blue and the red curves are the adapted coefficients of the controllers.

5.3.2 Simulation with a slower trajectory

We investigate if the translational motion of the object depends on the desired trajectory of the angular position of the object. The simulation is performed with the same parameters as before seen in Table 5.1 and 5.2, but the desired trajectory of the objects' orientation is chosen much slower.

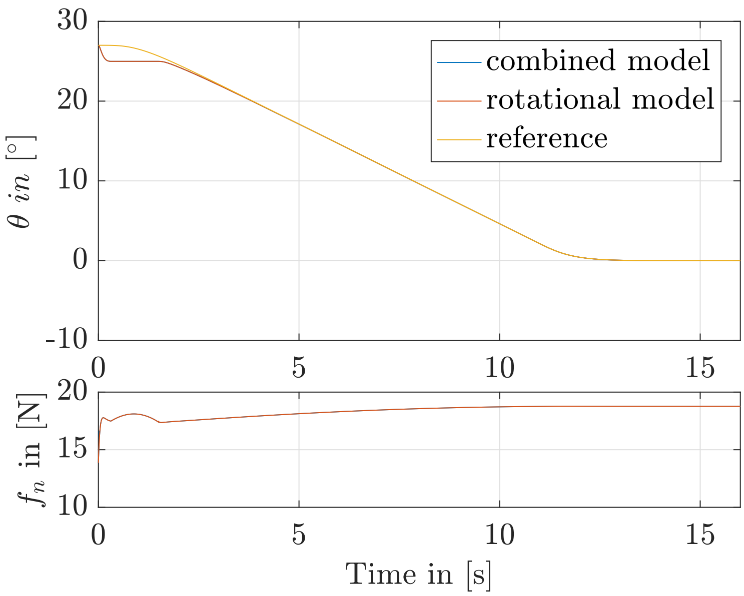

Figure 5.10: Angle of the object for the rotational and the combined model and the changed desired reference trajectory. The second plot shows the applied normal force during the pivoting process for both models.

Figure 5.10 shows the new reference trajectory and the simulated angular position of the object and the applied normal force for both models. We can see, that both models behave equal and the object follows the desired trajectory very well except to the beginning, which is attributed to the wrong initial torsional friction coefficient of the controller.

The translational motion and the adaption of the torsional friction coefficient can be seen in Fig. 5.11. The total displacement in y-direction for both models is with around -0.043 mm the same as for the faster trajectory in Section 5.3.1. Therefore, we assume that the translational motion does not or only little depend on the time the pivoting requires.

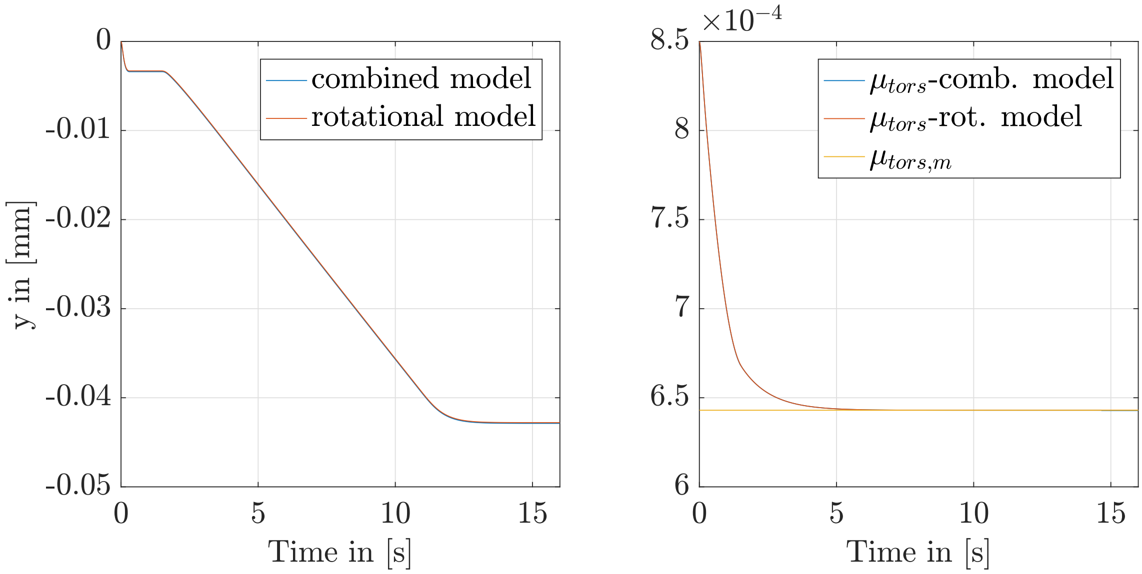

Figure 5.11: Adaptation of the torsional friction coefficient for the controller of the rotational and the combined model during pivoting. The yellow line is the coefficient, which is used by the contact models, while the blue and the red curves are the adapted coefficients of the controllers.

The adaptation of the torsional friction coefficient is also comparable to the section before. At around 5 seconds, the adaptation reaches the torsional friction coefficient of the contact model.

5.3.3 Simulation with modified object parameters

The object parameters get changed, such that the ratio of gravitational force to the gravitational torque becomes bigger compared to the simulations before. The parameters of the contact and object model can be seen in Table 5.3. The parameters of the controller remain the same and can be obtained from Table 5.2. Only the desired object orientation is set to $\theta_d = -80°$.

Table 5.3: Changed parameters of the object and contact model.

g [m/s^2]	9.81
m [g]	592.7
l_{center} [cm]	1
I [Kg $\cdot$ cm^2]	0.79
γ	0.3
μ	0.47
$\mu_{tors,m}$	0.85 $\cdot 10^{-3}$
θ_0 [°]	-25

The object length is set around 12 times smaller than in the scenarios before. To keep the applied normal force in the same range as before, the object mass is set bigger with the same factor. Therefore, the gravitational torque remains the same for the same angular position of the object. However, the gravitational force is around 12 times bigger now. The moment of inertia of the object to the grasping point is approximated with $I = \frac{1}{3}ml^2$ where $l = 2l_{center}$, which corresponds the the moment of inertia of a thin rod.
Figure 5.12 shows the angular position of the rotational and the combined model and the reference trajectory, as well as the normal force which is applied to the object for each model.

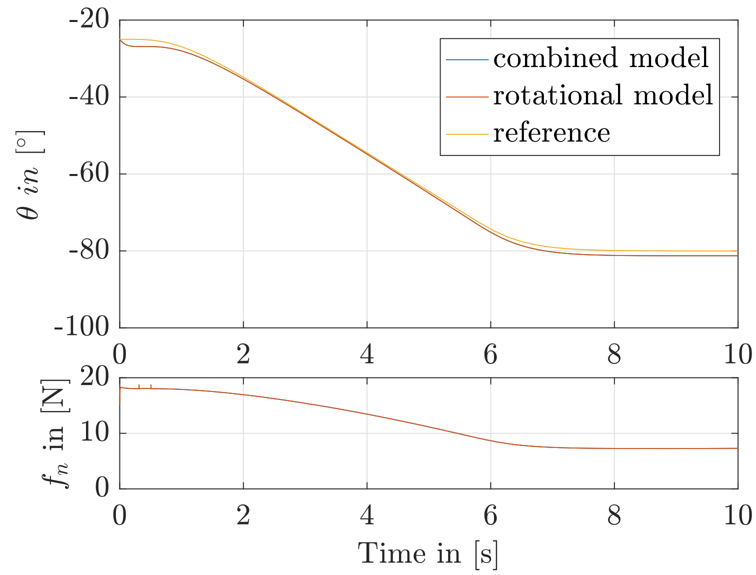

Figure 5.12: Angle of the object for the rotational and the combined model and desired reference angle for changed object parameter seen in Table 5.3. The second plot shows the applied normal force during the pivoting process for both models.

Both models behave the same and can follow the desired trajectory quite well, however, the angular position overshoots the desired orientation about 1.5°. The applied normal force of both models is very similar during the whole process.
Figure 5.13 illustrates the parameters h_{comb}, h_{rot}, b_{comb} and b_{rot} for the changed object parameters. The assumption that the parameters are slow varying during

the in-hand manipulation task is not valid anymore. Especially, h_{rot} and b_{rot} of the rotational model change more than twice of their initial value during the time.

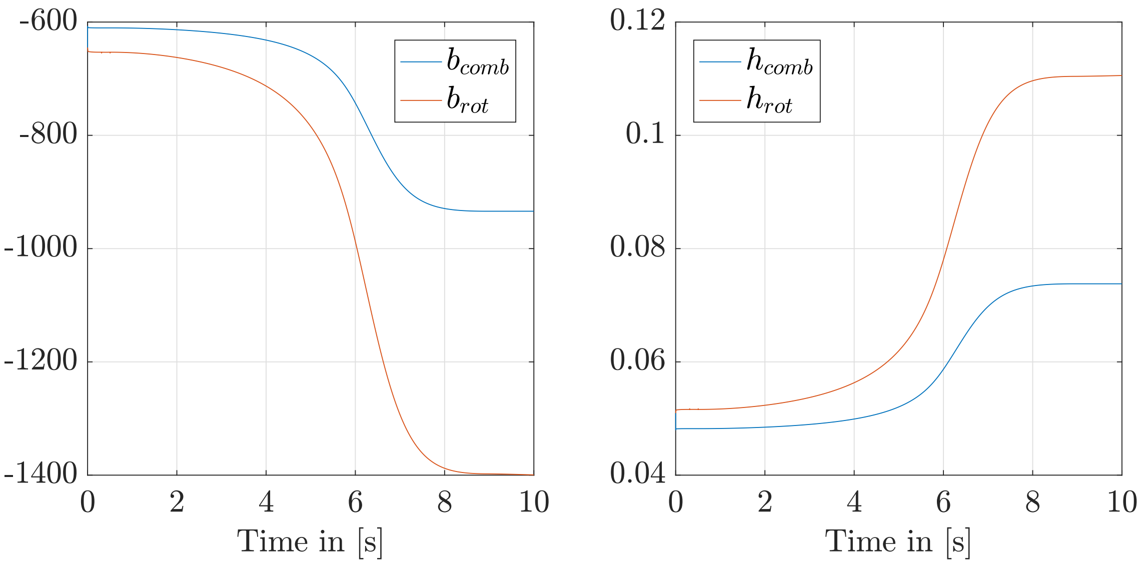

Figure 5.13: Parameters b_{comb} and h_{comb} of the combined model and b_{rot} and h_{rot} of the rotational model during pivoting.

The estimated parameters $\hat{b}_{comb}$ and $\hat{h}_{comb}$ of the combined model and $\hat{b}_{rot}$ and $\hat{h}_{rot}$ of the rotational model can be seen in Fig. 5.14. It can be noted that $\hat{b}_{comb}$ and $\hat{b}_{rot}$ do not converge to any value. This can be attributed to the fact, that the angular position has a steady state error and the adaptation law (4.11) depend on the tracking error.

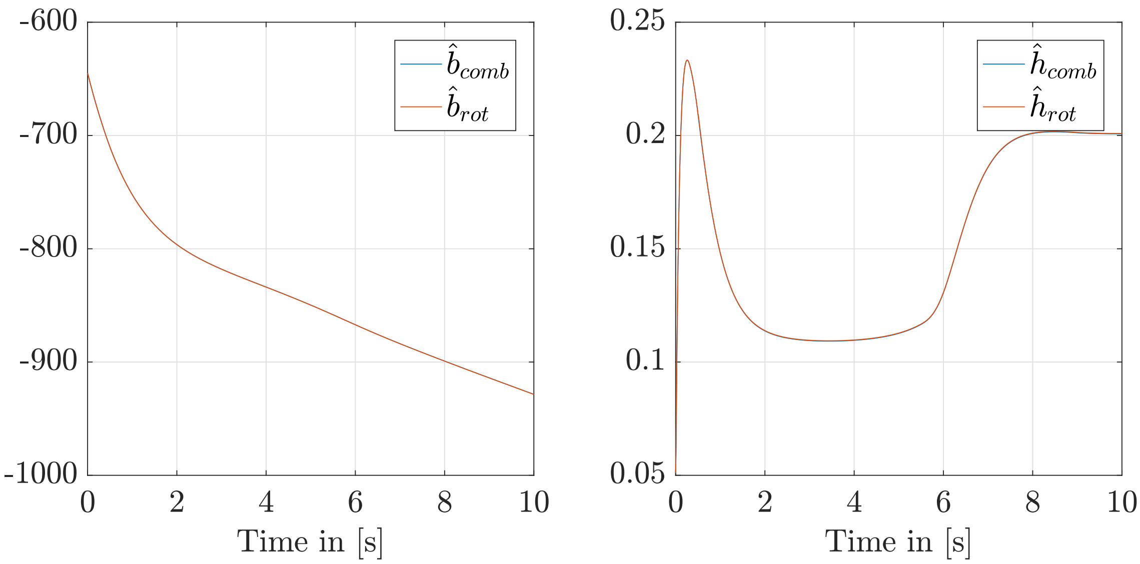

Figure 5.14: Estimation of $\hat{b}_{comb}$ and $\hat{h}_{comb}$ of the combined model and $\hat{b}_{rot}$ and $\hat{h}_{rot}$ of the rotational model during pivoting.

Figure 5.15 shows the movement in y-direction of the object and the adaptation of the torsional friction coefficient for both models.

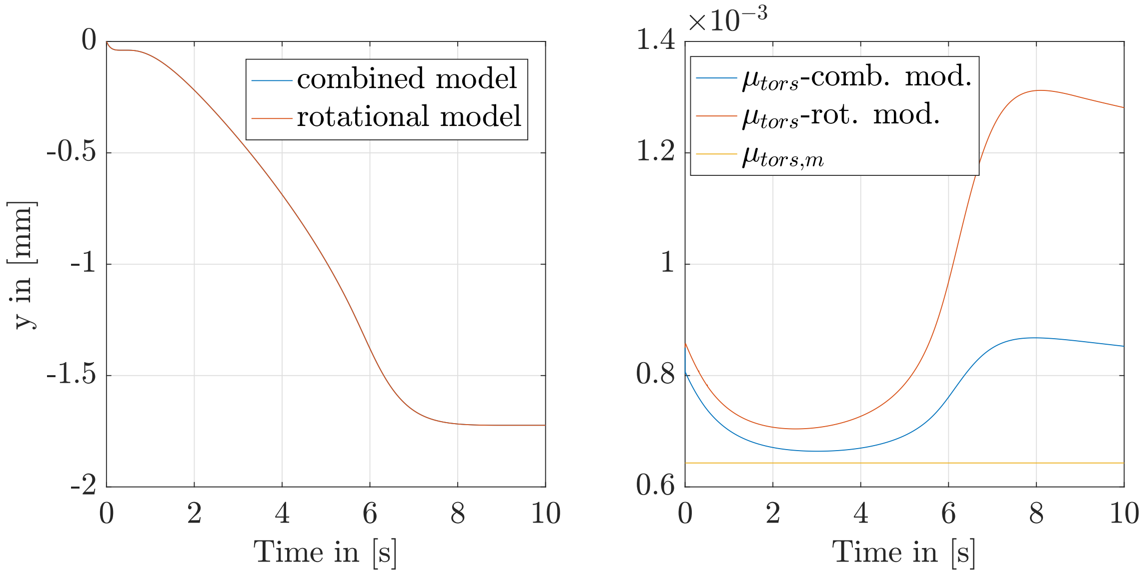

Figure 5.15: Adaptation of the torsional friction coefficient for the controller of the rotational and the combined model during pivoting. The yellow line is the coefficient, which is used by the contact models, while the blue and the red curves are the adapted coefficients of the controllers.

The displacement of the object for the combined model is bigger than for the rotational model. This can be expected since the angular position has an overshooting (Fig. 5.12) and therefore, a bigger change. It is also notable that the translational movement is more than 30 times bigger than in the scenario before (Fig. 5.9). The torsional friction coefficient of the controllers cannot be adapted to the real coefficient of the contact models. However, as in Section 4.1 explained, a convergence is not guaranteed. To conclude, the assumption of slow varying parameters h_{comb}, h_{rot}, b_{comb} and b_{rot} is not full filled for this scenario. However, the controller can still manage to follow the desired trajectory quite well. The steady state error of both models is around 1.5°.

5.4 Model free control

Now the model free controller of Section 4.2 is utilized. Since both contact models have been investigated before and the results can be seen as nearly identical for the pivoting tasks, only the more advanced model, the combined model is considered here. The object parameters are shown in Table 5.1 again and the additional parameters for the predefined bounds, the reference trajectory and the model free controller can be seen in Table 5.4.

Table 5.4: Parameters for the pivoting with the model free controller.

ρ_0	1
ρ_∞	0.05
l	0.8
M	0.5
K_{mf}	0.08
θ_d [°]	0
λ	10
λ_0	2.5

The control gain K_{mf} is chosen with the knowledge we got from the previous experiments with the adaptive controller. Since we want to achieve a very small steady state error, the normal force for $s = 0$ should be close to the steady state normal force of Fig. (5.6). Together with the chosen parameter M, ρ_∞ and Eq. (4.16) we can estimate $K_{mf} = 0.08$.

Figure 5.16 shows the angular position of the object and the normal force during pivoting. The model free controller can follow the trajectory very well with a small error in the beginning, which is comparable to the adaptive controller shown in 5.6.

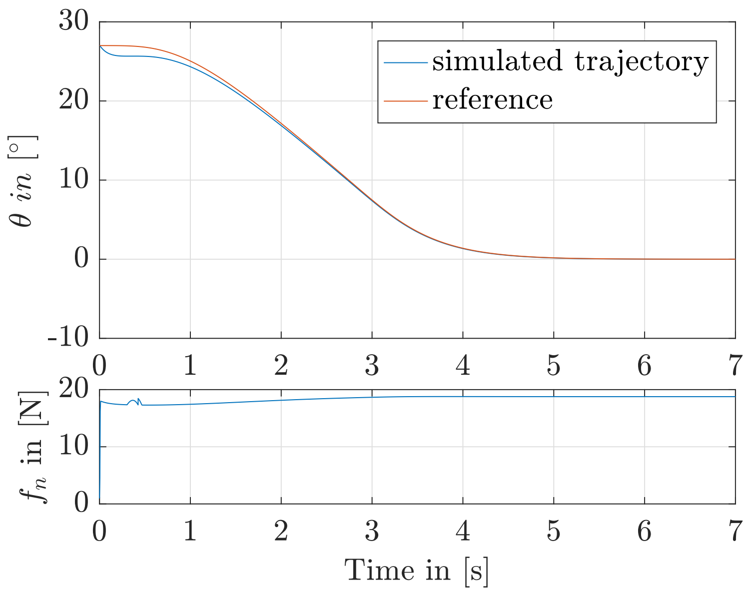

Figure 5.16: Angle of the object for the combined model utilizing the model free controller, desired reference angle and normal force which is applied from the fingertips to the object.

The translational displacement in y-direction and the error bounds with the normalized combined error is illustrated in Fig. 5.17.

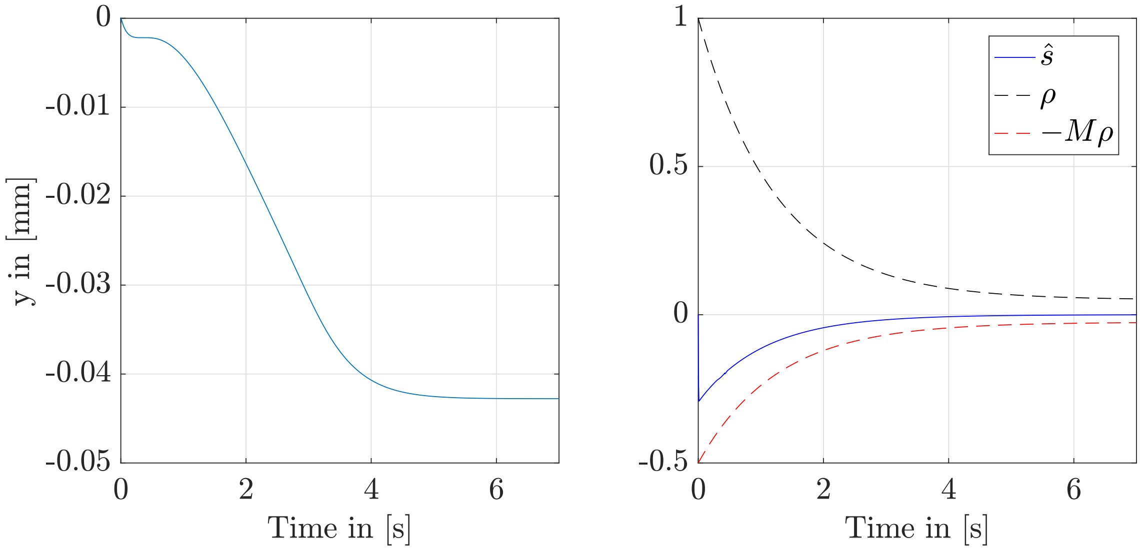

Figure 5.17: Translational motion in y-direction for the combined model with the model free controller and normalized error $\hat{s}$ with the predefined error bounds.

The shape of the translational motion follows the shape of the trend of the angular position. Therefore, the curve looks the same as the translational motion of the adpative controller in Fig. 5.9. The normalized error starts at zero, jumps to -0.3 and converges after that to zero. This is expected since the angular position starts at the right value, has an error after that, but converges to the desired angular position.

5.4.1 Simulation with modified object parameters

By changing the object parameters to the values proposed in Table 5.3 and setting the desired angular end position of the object to $\theta_d = -80°$, we can compare the model free controller to the adaptive controller, which results are shown in Section 5.3.3. The control gain is set accordingly to the steady state normal force of Fig. 5.12 to $K_{mf} = 0.04$. The angular position and the normal force during pivoting can be seen in Fig. 5.18. Compared to the adaptive controller shown in Fig. 5.12, the angular position has a similar error in the first second. However, the angular position does not overshoot the desired end angle.

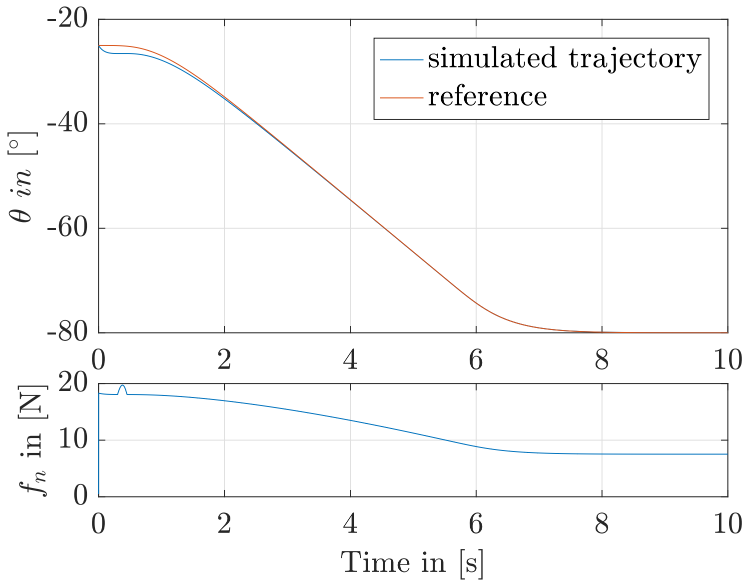

Figure 5.18: Angle of the object for the combined model utilizing the model free controller, desired reference angle and normal force which is applied from the fingertips to the object.

The translational motion seen in Fig 5.19 is very similar to the adaptive controller (Fig. 5.15). Only the total displacement is less, which can be attributed to the fact that the angular position of the model free controller does not overshoot. The normalized error is compared to the scenario before a little bigger in the beginning. This can be explained since the controller is optimized for a possibly small steady state error. Because the needed normal force in the beginning of the process is more than twice as big as at the end we get a relatively big error in the beginning.

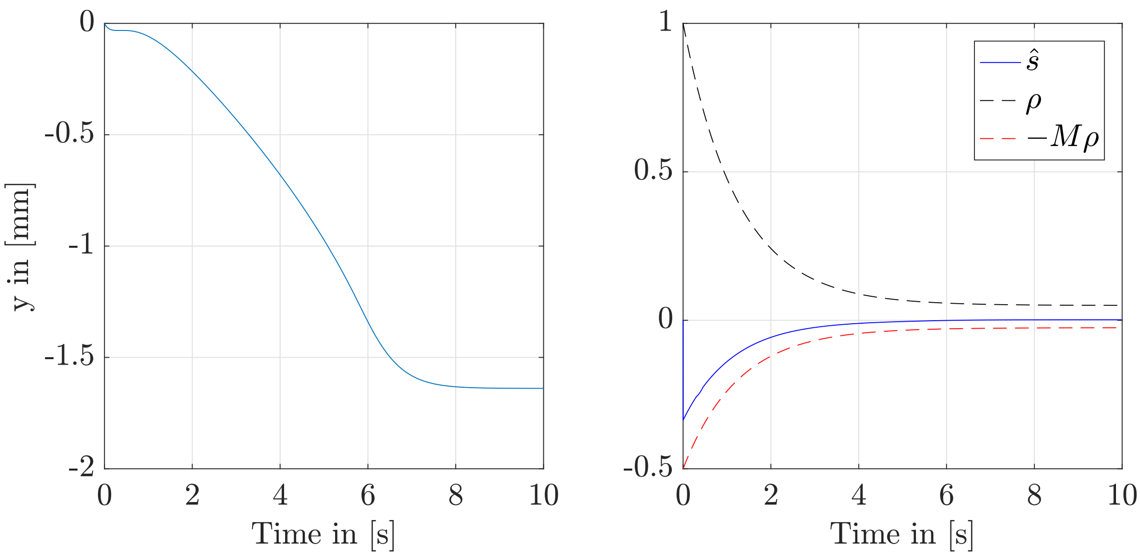

Figure 5.19: Translational motion in y-direction for the combined model with the model free controller and normalized error $\hat{s}$ with the predefined error bounds.

5.4.2 Pivoting without a reference trajectory

In-hand manipulation without a reference trajectory is performed with the model free controller proposed in Section 4.2 where the tracking error e defined in (4.18) is utilized. The object parameters of Table 5.1 are applied and the parameters for the controller and the prescribed error bounds are shown in Table 5.5.

Table 5.5: Parameters for the pivoting with the model free controller without a reference trajectory.

ρ_0	6
ρ_∞	0.05
l	1.5
M	0
K_{mf}	0.05
θ_d [°]	0
λ	3

The results for this simulation scenario are shown for both the rotational and the combined model. The angular position and the applied normal force for both models can be seen in Fig. 5.20. Since we do not have a reference trajectory, the angular position is changing faster in the beginning and then converges to the desired orientation. Both models have again the same behavior and no overshoot. The normal force increases very fast in the beginning and then stays nearly constant.

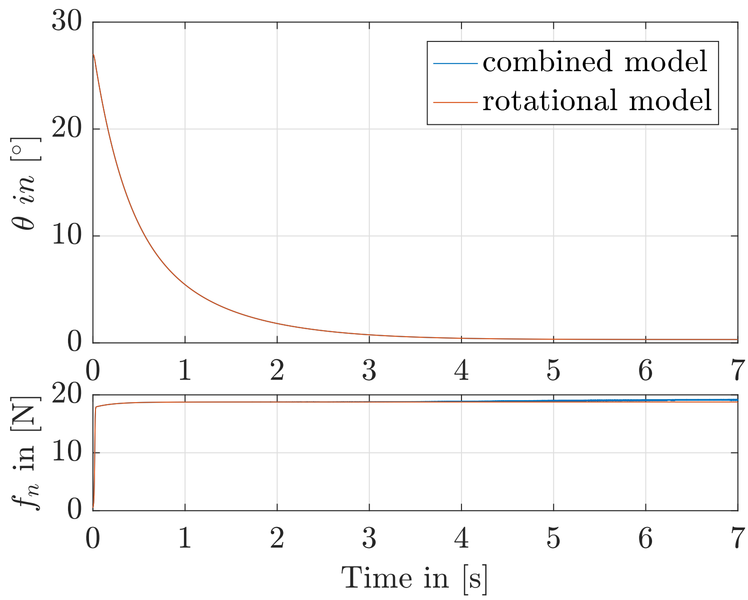

Figure 5.20: Angle of the object for the rotational and the combined model utilizing the model free controller without a reference trajectory and normal force which is applied from the fingertips to the object.

The displacement in y-direction shown in Fig. 5.21 shows different results for both models. The rotational model ends up at $-0.042\,\text{mm}$ which is comparable to the result of the pivoting with a reference trajectory (Fig. 5.17). For the combined model, the object moves around -0.002 mm further. This corroborate the statement that the translational motion of both models behave different for fast velocities. As in Section 3.2 proposed, the combined model can be seen as more reliable for these cases.

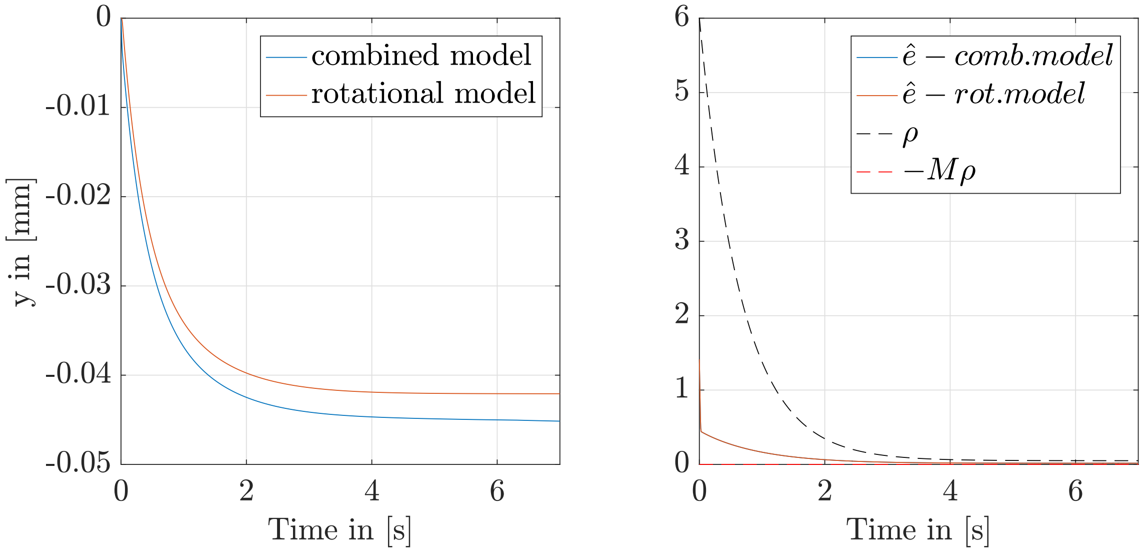

Figure 5.21: Translational motion in y-direction for both models with the model free controller without a reference trajectory and normalized error $\hat{e}$ with the pre-defined error bounds.

The normalized error for both models starts at 1.4 and decreases very fast caused by the high velocity and then converges to zero. However, it has to be noticed that $\hat{e}$ cannot reach zero because we chose $M = 0$ and therefore, the normal force would be infinity for $\hat{e} = 0$ accordingly to (4.15) and (4.16). Therefore, we always get a positive steady state error for the angular position.

To conclude this chapter, the rotational and the combined model have been evaluated as nearly identical. Only for pivoting without a reference trajectory the translational motion is different for both models, which can be traced back to the much higher velocities for this scenario. In this case the more reliable model, the combined model, has a slightly bigger displacement in y-direction, which is also bigger than the tranlational motion for the same scenario with a reference tracking. Therefore, it is desirable to pivot with a reference trajectory or penalize the rotational velocity more to guarantee a smallest possible translational motion. Both control approaches have shown good results for the in-hand manipulation task where the gravitational torque is much bigger than the gravitational force. If this is not full filled the adaptive controller cannot successfully estimate the torsional friction coefficient and overshoots the desired angular orientation. The model free controller showed even for this scenario very good trajectory tracking without overshooting the desired orientation.

6
Conclusion and Future Work

In-hand manipulation with the help of gravity is aimed for this thesis. A one degree of freedom parallel jaw gripper was considered to grasp the object in such way, that the orientation of the object can be controlled in a desired manner. This is achieved through precises controlling of the grasping force. To simulate this process, an accurate model is required that covers the contact between the fingertips of the gripper and the object.
Two different contact models have been considered. Both models are based on the concept of the limit surface, which was first introduced by Goyal et al. [15]. The concept of the limit surface describes the relation between translational and rotational friction forces and torques and the corresponding dynamics.
The first contact model, the rotational model, uses the concept of the limit surface to directly calculate the frictional torque for the rotational dynamics. The translational velocity is then approximated with a ratio consisting of external forces and torques applied to the object and the maximal frictional force and torque, which can be independently resisted by the contact. The second contact model, the combined model, uses a friction force vector to calculate both the rotational and the translation dynamics. The friction force vector depends on the actual velocities of the object and on the constructed limit surface.
Comparisons of both models have shown a very similar behavior for the rotational movements of the object. However, the translational motions differ. For the shown test cases, the rotational model demonstrate a bigger translational movement compared to the combined model if the orientation of the object is close to $-90°$, which corresponds to a low gravitational torque. In other cases it is vice versa. This variation can be attributed to the reason that the rotational model does not calculate translational dynamics, but it approximates the translational velocity depended on the rotational velocity. Therefore, we trust the results of the combined model more than the results of the rotational model.

To change the orientation of the object in a desired way, different control approaches were considered. Since the torsional friction coefficient was seen as uncertain, a nonlinear adaptive controller was used. The adaptive controller was introduced by Viña B. et al. [6] and estimates the torsional friction coefficient. However, the utilized control theory does not apply exactly to the contact models. Therefore, its validity was shown through simulation. Another control approach to handle the unknown torsional friction coefficient is a model free controller with prescribed performance guarantees, which was proposed by Karayiannidis et al. [10]. Since we can only apply a positive normal force to the object, the control input is limited and we had

to find a suitable error transformation function, which maps the tracking error such that we get a positive normal force.
The evaluation of both control approaches combined with both contact models pointed out that both contact models behave the same if the velocities are reasonable slow. If the gravitational torque is much bigger than the gravitational force both control approaches can reach the control goals. If this is not given, the adaptive controller misses the control goal by slightly overshooting the desired orientation. The model free controller can still achieve a very good trajectory tracking. Pivoting without a reference trajectory was performed with the model free controller and pointed out as a valid control strategy since the desired angular orientation was reached. However, the translational displacement was slightly higher in this scenario, which was caused by the high velocities. Other scenarios showed that a slower reference trajectory cannot shrink the translational motion. Therefore, we conclude, that the displacement in y-direction is independend of the pivoting speed, as long as the velocities are not too high.

All in all a powerful simulation model was created, which can be improved more in future work. The contact models and the controllers can be compared to experimental data gathered from sensors while performing in-hand manipulation with a robot. This will show the accuracy of the models and their power to predict and investigate the process. The use of elasto-plastic models may improve the accuracy of the contact model, since it covers stiction, presliding displacement and sliding. This class of friction models is presented e.g. in [25] and [26]. Another possible extension to the presented work is including other extrinsic dexterities except of the gravity. For example, the object could make external contact to a surface to perform active pivoting and enable other in-hand manipulation tasks.

Bibliography

[1] N. Dafle and A. Rodriguez, "Prehensile pushing: In-hand manipulation with push-primitives", *IEEE/RSJ International Conference on Robotic and Automation* 2015.

[2] N. Dafle, A. Rodriguez, R. Paolini, B. Tang, S. Srinivasa, M. Erdmann, M. Mason, I. Lundberg, H. Staab, and T. Fuhlbrigge, "Extrinsic dexterity: In-hand manipulation with external forces", *IEEE International Conference on Robotic and Automation*, pp. 1578–1585, May 2014.

[3] A. Holladay, R. Paolini, and M. Mason, "A general framework for open-loop pivoting", *IEEE International Conference on Robotic and Automation*, pp. 3675–3681, May 2015.

[4] J. Shi, Z. Woodruff, and K. M. Lynch, "Dynamic in-hand sliding manipulation", *IEEE/RSJ International Conference on Robotic and Automation* 2015.

[5] F. E. Viña B., Y. Karayiannidis, K. Pauwels, C. Smith, and D. Kragic, "In-hand manipulation using gravity and controlled slip", *IEEE/RSJ International Conference on Intelligent Robots and Systems* 2015.

[6] F. E. Viña B., Y. Karayiannidis, C. Smith, and D. Kragic, "Adaptive Control for Pivoting with Visual and Tactil Feddback" 2016.

[7] R. D. Howe and M. R. Cutkosky, "Practical force-motion models for sliding manipulation", *The international Journal of Robotics Research*, vol. 15, no. 6, pp. 557–572, 1996.

[8] N. Xydas and I. Kao, "Modeling of Contact Mechanics and Friction Limit Surfaces for Soft Fingers in Robotics, with Experimental Results", *The International Journal of Robotic Research*, vol. 18, no. 9, pp. 941–950, Sept. 1999.

[9] J. Slotine and W. Li, *Applied Nonlinear Control*, Prentice Hall, 1991.

[10] Y. Karayiannidis, D. Papageorgiou, and Z. Doulgeri, "A model-free controller for guaranteed prescribed performance tracking of both robot joint positions and velocities", *IEEE Robotics and Automation Letters*, vol. 1, no. 1 Jan. 2016.

[11] H. Liu, K.C. Nguyen, V. Perdereau, J. Bimbo, J. Back, M. Godden, L. D. Seneviratne, and K. Althoefer, "Finger contact sensing and the application in dexterous hand manipualtion", *Journal of Applied Mechanics*, vol. 39, pp. 25–41, 2015.

[12] Andrea Bisoffi, Mauro Da Lio, Andrew R. Teel, and Luca Zaccarian, "Global asymptotic stability of a PID control system with Coulomb friction" June 2002.

[13] S. R. Dahmen, Z. Farkas, H. Hinrichsen, and D. E. Wolf, "Macroscopic diagnostics of microscopic friction phenomena", *Physical Review E71* 2005.

[14] Zénó Farkas, G. Bartels, T. Unger, and D. E. Wolf, “Frictional Coupling between Sliding and Spinning Motion”, *Physical Review Letters*, vol. 90, no. 24 June 2003.

[15] S. Goyal, A. Ruina, and J. Papadopoulos, “Planar sliding with dry friction, part 1. Limit surface and moment function”, *Wear*, vol. 143, pp. 307–330, 1991.

[16] S. Goyal, “Planar sliding of a rigid body with dry friction: limit surface and dynamics of motion”, PhD thesis, Cornell University, Jan. 1989.

[17] K. L Johnson, *Contact mechanics*, Cambridge, UK: Cambridge University Press, 1985.

[18] H. Hertz, “On the Contact of Rigid Elastic Solids ans on Hardness”, in: New York: Macmillan, 1882, chap. 6.

[19] J. W. Hutchinson, “Fundamentals of the phenomenological theory of nonlinear fracture mechanics”, *Journal of Applied Mechanics*, vol. 105, no. 50, pp. 1042–1051, 1983.

[20] C. Bechlioulis and G. Rovithakis, “Robust adaptive control of feedback linearizable MIMO nonlinear systems with prescribed performance”, *IEEE Transactions on automatic control*, vol. 53, no. 9, pp. 2090–2099, Oct. 2008.

[21] Y. Karayiannidis and Z. Doulgeri, “Model-free robot joint position regulation and tracking with prescribed performance guarantees”, *Robotics and Autonomous Systems*, vol. 60, no. 2, pp. 228–235, 2012.

[22] Y. Karayiannidis, V. Dimarogonas, and D. Kragic, “Multi-agent average consensus control with prescribed performance guarantees”, *IEEE Conference on Decision and Control*, vol. 51, pp. 2219–2225, Dec. 2012.

[23] D. Kubus, T. Kröger, and F. M Wahl, “On-line rigid object recognition and pose estimation based on inertial Parameters”, *IEEE/RSJ International Conference on Intelligent Robots and Systems*, pp. 1402–1408, Oct. 2007.

[24] R. C. Dorf and R. H Bishop, *Modern control systems*, vol. 12, Prentice Hall, 2011.

[25] P. Dupont, B. Armstrong, and V. Hayward, “Elasto-Plastic Friction Model: Contact Compliance and Stiction”, *AACC* June 2000.

[26] P. Dupont, V. Hayward, B. Armstrong, and F. Altpeter, “Single State Elasto-Plastic Friction Models”, *IEEE Transactions on Automatic Control* June 2002.

A

Appendix

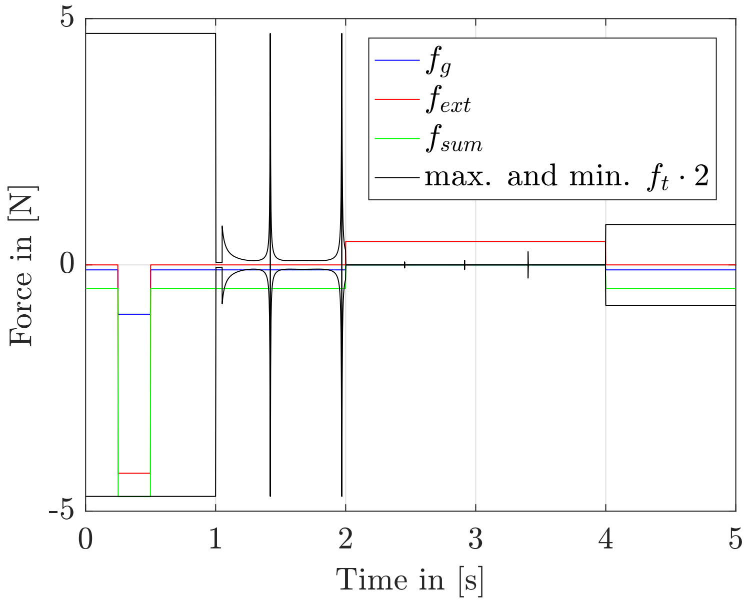

Figure A.1: Occurring forces while pivoting with an external force and torque for the rotational model. The black lines are the minimal and maximal frictional forces caused by a gripping force of 5 N.

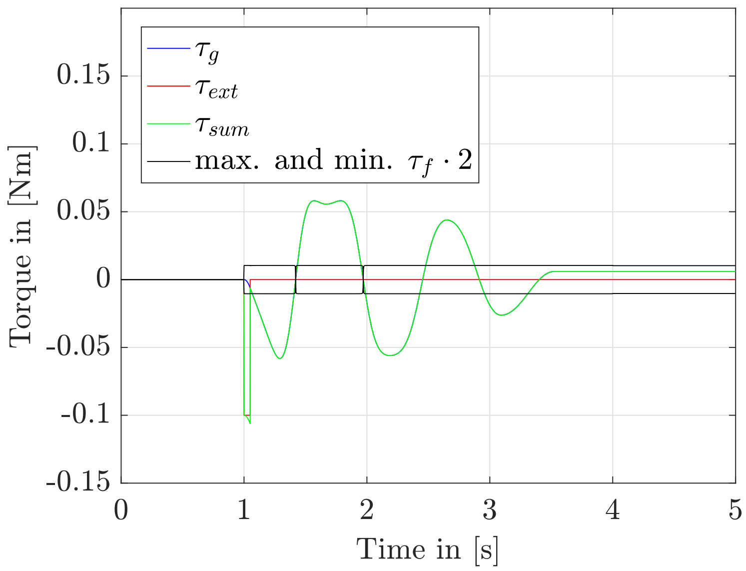

Figure A.2: Occurring torques while pivoting with an external force and torque for the rotational model. At 1 second a negative external pulse is given. After that, $\tau_{sum} = \tau_g$. The black lines are the minimal and maximal frictional torques caused by a gripping force of 5 N.